UNICAMP

UNIVERSIDADE ESTADUAL DE CAMPINAS
Faculdade de Engenharia Mecânica

Pedro Gatti Artaxo Netto

Flight Control for Target Tracking with Multiple Coordinated Airships

Controle de Voo Coordenado para Rastreamento de Alvo com Múltiplos Dirigíveis

CAMPINAS
2018

Pedro Gatti Artaxo Netto

Flight Control for Target Tracking with Multiple Coordinated Airships

Controle de Voo Coordenado para Rastreamento de Alvo com Múltiplos Dirigíveis

Dissertation presented to the Faculty of Mechanical Engineering of the University of Campinas in partial fulfillment of the requirements for the degree of Master in Mechanical Engineering, in the area of Mechatronics.

Dissertação de Mestrado apresentada à Faculdade de Engenharia Mecânica da Universidade Estadual de Campinas como parte dos requisitos exigidos para obtenção do título de Mestre em Engenharia Mecânica, na Área de Mecatrônica.

Orientador: Prof. Dr. Ely Carneiro de Paiva

ESTE EXEMPLAR CORRESPONDE À VERSÃO FINAL DA DISSERTAÇÃO DEFENDIDA PELO ALUNO Pedro Gatti Artaxo Netto, E ORIENTADO PELO PROF. DR Ely Carneiro de Paiva.

....
ASSINATURA DO ORIENTADOR

CAMPINAS
2018

Agência(s) de fomento e nº(s) de processo(s): CAPES, 1687527; CAPES, 1784708
ORCID: https://orcid.org/0000-0003-2921-127

Ficha catalográfica
Universidade Estadual de Campinas
Biblioteca da Área de Engenharia e Arquitetura
Luciana Pietrosanto Milla - CRB 8/8129

	Artaxo Netto, Pedro Gatti, 1991-
Ar75f	Flight control for target tracking with multiple coordinated airships / Pedro Gatti Artaxo Netto. – Campinas, SP : [s.n.], 2018.
	Orientador: Ely Carneiro de Paiva.
	Dissertação (mestrado) – Universidade Estadual de Campinas, Faculdade de Engenharia Mecânica.
	1. Robótica. 2. Robos - Sistemas de controle. 3. Voo - Controle. 4. Sistemas de veículos auto-guiados. 5. Monitoramento ambiental. I. Paiva, Ely Carneiro de, 1965-. II. Universidade Estadual de Campinas. Faculdade de Engenharia Mecânica. III. Título.

Informações para Biblioteca Digital

Título em outro idioma: Controle de voo coordenado para rastreamento de alvo com múltiplos dirigíveis
Palavras-chave em inglês:
Robotics
Robots - Control systems
Flight - Control
Self-guided vehicle systems
Environmental monitoring
Área de concentração: Mecatrônica
Titulação: Mestre em Engenharia Mecânica
Banca examinadora:
André Ricardo Fioravanti
Grace Silva Deaecto
Matheus Souza
Data de defesa: 05-04-2018
Programa de Pós-Graduação: Engenharia Mecânica

UNIVERSIDADE ESTADUAL DE CAMPINAS
FACULDADE DE ENGENHARIA MECÂNICA
COMISSÃO DE PÓS-GRADUAÇÃO EM ENGENHARIA MECÂNICA
DEPARTAMENTO DE SISTEMAS INTEGRADOS

DISSERTAÇÃO DE MESTRADO

Flight Control for Target Tracking with Multiple Coordinated Airships

Controle de Voo Coordenado para Rastreamento de Alvo com Múltiplos Dirigíveis

Autor: Pedro Gatti Artaxo Netto

Orientador: Prof. Dr. Ely Carneiro de Paiva

A Banca Examinadora composta pelos membros abaixo aprovou esta Dissertação:

Prof. Dr. André Ricardo Fioravanti
Instituição: FEM/UNICAMP

Profa. Dra. Grace S. Deaecto
Instituição: FEM/UNICAMP

Prof. Dr. Matheus Souza
Instituição: FEM/UNICAMP

A Ata da defesa com as respectivas assinaturas dos membros encontra-se no processo de vida acadêmica do aluno.

Campinas, May 23, 2018

Agradecimentos

Começo agradecendo ao professor Dr. Ely Carneiro de Paiva pela orientação, não apenas científica, tanto durante o curso de graduação, como neste mestrado.

Agradeço ao Dr. Samuel Siqueira Bueno e ao Prof. Dr. José Raul Azinheira, pelas críticas e sugestões extremamente pertinentes que ajudaram que este trabalho se tornasse melhor do que era.

Agradeço aos professores que tive, que tanto me ensinaram quanto se tornaram modelos do profissional que eu desejo ser.

Agradeço muito à minha família, que sempre me deu - e tenho certeza que sempre dará - apoio incondicional em todos os momentos da minha vida, não importando as circunstâncias. Particularmente aos meus pais, que não só puderam prover uma orientação acadêmica, como me proporcionaram condições para conquistar meus sonhos, em um país que tem na "meritocracia" uma cortina que encobre a desigualdade de oportunidades.

Agradeço também aos meus amigos, pois sem eles todo este percurso seria muito mais difícil e, possivelmente, nunca terminado.

Por fim, agradeço a CAPES pelo suporte financeiro durante meu mestrado.

Nenhum país pode realmente desenvolver-se a menos que os seus cidadãos sejam educados.

Nelson Mandela

Resumo

Este trabalho propõe e executa o desenvolvimento, em simulação, de um sistema de controle de voo em formação de três dirigíveis para o rastreamento de alvos móveis em solo. A primeira etapa do trabalho envolve a adaptação do simulador dinâmico do dirigível pré-existente em software Simulink/Matlab para um cinemático, além da implementação de sistemas de controle de voo cooperativo do tipo líder-seguidor para percorrer um dado trajeto. Na sequência, foram projetados e implementados algoritmos de controle de voo em formação para os três dirigíveis perseguindo um alvo em solo, com formação em diagonal ("V"), ou alinhados lateral, ou longitudinalmente. Finalmente, as técnicas desenvolvidas foram aplicadas no simulador dinâmico do dirigível, onde se continuou o desenvolvimento do trabalho para uma implementação satisfatória. A abordagem utilizada envolve dois laços de controle, onde o externo faz controle de posição e o interno faz o controle dinâmico. O laço externo é constituído de um controlador linear cinemático e algoritmos para planejamento de trajetória e coordenação entre os dirigíveis. O laço interno é um controlador por modos deslizantes com um escalonador de ganhos acoplado, melhorando a aplicação já existente desse controlador. Várias abordagens de rastreamento desse tipo já foram propostas e testadas para aeronaves convencionais, mas o autor desconhece uma aplicação assim para o voo coordenado de dirigíveis. O trabalho se insere no contexto de três projetos de pesquisa em andamento, sendo um deles o Projeto Temático "INCT em Sistemas Autônomos Cooperativos" (FAPESP: 2014/50851-0 e CNPq: 465755/2014-3). As plataformas robóticas alvo deste trabalho são os dirigíveis do Projeto DRONI – CNPq e do Projeto Temático INCT, uma aeronave instrumentada de 10 m de comprimento com quatro propulsores elétricos. As aplicações principais desse trabalho estão voltadas para o monitoramento e vigilância na região amazônica, através de uma parceria existente com a UFAM e com o Instituto Mamirauá (IDSM), onde se pretende utilizar, futuramente, o voo cooperativo para vigilância e rastreamento de alvos móveis.

Palavras-chave: Veículos Aéreos Não Tripulados; Robótica móvel; Monitoramento ambiental; Dirigíveis.

Abstract

The following work proposes and executes the development, in a simulated environment, of a coordinated flight control system of three airships, focusing on environmental monitoring and surveillance. The first part of this work involved the adaptation of the preexisting dynamical airship simulator, in Simulink/Matlab, to a kinematic, besides the implementation of control systems for cooperative flight, of the leader-follower kind, to follow a given trajectory. Furthermore, algorithms for the cooperative flight control for tracking a ground target were designed and implemented, in “V” formation or aligned. Finally, the developed techniques were applied in the dynamic simulator, where the development continued to achieve a satisfactory performance. The approach utilized involves two control loops, where the external controls the position and the internal controls the airship dynamics. The external loop consists of a state-feedback kinematic controller and algorithms for trajectory planning and coordination between the airships. The internal loop is a sliding mode controller with a coupled Gain Scheduler, enhancing the existing application of that controller. Several approaches for this kind of tracking were proposed and tested for conventional aircraft so far, but none for coordinated airships, as far as the author knows. The work is a part of three ongoing research projects, one being the Thematic Project “INCT em Sistemas Autônomos Cooperativos” (FAPESP: 2014/50851-0 e CNPq: 465755/2014-3). The targeted robotic platforms are the airships from the DRONI project - CNPq and Thematic Project INCT, a 10 m long instrumented aircraft, with four electric propulsors. As said, the main applications for this work revolve around monitoring and surveillance in the Amazon region, through an existing partnership with UFAM and Mamirauá Institute (IDSM), where it is intended to use the cooperative flight for monitoring and mobile-target tracking.

Keywords: Unmanned aerial vehicles; Mobile robots; Environmental monitoring; Airships.

List of Figures

List of Tables

List of Symbols

Sign	Description	Unit
$\boldsymbol{\Phi}$	Airship (NED frame): Angular attitude in euler angles - $\boldsymbol{\Phi} = [\varphi\ \theta\ \psi]^{\mathrm{T}}$	rad
$\mathit{\Psi}$	Chattering smoothing for the sliding mode control	
$\boldsymbol{\Omega}$	Cross-product matrix equivalent to $\boldsymbol{\omega}\times$	rad/s
δ	Current sent to the electric motor. The subscript designates which and if its for the vectorization or rotor feed.	A
$\boldsymbol{\eta}$	Airship (NED frame): Complete position vector - $\boldsymbol{\eta} = [\mathbf{p}^{\mathrm{T}},\ \mathbf{q}^{\mathrm{T}}]^{\mathrm{T}}$	
$\boldsymbol{\nu}$	Airship (NED frame): Complete position vector - $\boldsymbol{\nu} = [\mathbf{p}^{\mathrm{T}},\ \boldsymbol{\Phi}^{\mathrm{T}}]^{\mathrm{T}}$	
σ	Switching function for the sliding mode control	
$\boldsymbol{\tau}$	General symbol for torque	N m
$\boldsymbol{\omega}$	Airship (ABC frame): Angular speed vector $\boldsymbol{\omega} = [p\ q\ r]^{\mathrm{T}}$	rad/s
$\mathbf{B}$	Buoyancy or upthrust force	N
$\mathbf{C}$	$\begin{bmatrix} I_3 & 0_3 \\ 0_{1,3} & 0_{1,3} \\ 0_3 & I_3 \end{bmatrix} \in \mathbb{R}^{7\times 6}$	
$\mathbf{D}$	$\begin{bmatrix} \mathbf{S}^{\mathrm{T}} & 0 \\ 0 & \frac{1}{2}\mathbf{Q} \end{bmatrix}$	
$\mathbf{E}$	$\begin{bmatrix} m_w I_3 \\ m\mathbf{C}_3 \end{bmatrix}$	
$\mathcal{F}$	Generalized force vector	
$\mathbf{G}$	$\begin{bmatrix} \mathbf{S}^{\mathrm{T}} & 0 \\ 0 & \mathbf{R} \end{bmatrix}$	
$\mathbf{J}$	Inertia matrix of the airship	$\mathrm{kg\,m^2}$
$\mathbf{K}$	$\frac{\partial}{\partial \boldsymbol{\nu}}\mathbf{G}^{-1}\dot{\boldsymbol{\nu}}$	
$\mathbf{M}$	Mass matrix of the airship	kg
$\mathcal{M}$	Generalized mass matrix	

Sign	Description	Unit
$\mathbf{Q}$	Unitary matrix that relates the airship system angular velocities to quaternions derivatives	
$\mathbf{R}$	$\begin{bmatrix} 1 & \sin\varphi\tan\theta & \cos\varphi\tan\theta \\ 0 & \cos\varphi & -\sin\varphi \\ 0 & \dfrac{\sin\varphi}{\cos\theta} & \dfrac{\cos\varphi}{\cos\theta} \end{bmatrix}$	
$\mathbf{S}$	$\begin{bmatrix} \cos\psi\cos\theta & \sin\psi\cos\theta & -\sin\theta \\ \cos\psi\sin\theta\sin\varphi - \sin\psi\cos\varphi & \sin\psi\sin\theta\sin\varphi + \cos\psi\cos\varphi & \cos\theta\sin\varphi \\ \cos\psi\sin\theta\cos\varphi + \sin\psi\sin\varphi & \sin\psi\sin\theta\cos\varphi - \cos\psi\sin\varphi & \cos\theta\cos\varphi \end{bmatrix}$	
$\mathcal{S}$	Sliding surface hyperplane matrix defined as $\mathcal{S} = \{x \in R^n \ : \ Sx = 0\}$	
$\mathbf{T}$	Matrix product $\mathbf{DC}$	
$\mathbf{V}$	$\mathbf{V}_3$ is the cross product matrix equivalent of $\mathbf{v}\times$ and $\mathbf{V}_6$ is $\begin{bmatrix} 0 & 0 \\ \mathbf{V}_3 & 0 \end{bmatrix}$	m/s
W	Kinectic Energy	J
$\mathbf{X}$	$\begin{bmatrix} \mathbf{x} \\ \mathbf{x}_w \end{bmatrix}$	
$\mathbf{c}$	Vector from the CV to the CG	
$\mathbf{f}$	Acting forces generated by the electric motors	N
$\mathbf{g}$	Gravity acceleration	$\mathrm{m/s^2}$
m	Mass of the airship	kg
$\mathbf{p}$	Airship (NED frame): Linear position vector - $\mathbf{p} = [p_N \, p_E \, p_D]$	m
$\mathbf{q}$	Airship (NED frame): Angular attitude in quaternions - $\mathbf{q} = [q_0 \ q_1 \ q_2 \ q_3]^{\mathrm{T}}$	
$\mathbf{u}$	Control input for the airship	
$\mathbf{v}$	Airship (ABC frame): Linear velocity $\mathbf{v} = [u \ v \ w]^{\mathrm{T}}$	m/s
$\mathbf{x}$	Velocity vector $[\mathbf{v}^{\mathrm{T}} \ \boldsymbol{\omega}^{\mathrm{T}}]^{\mathrm{T}}$	

List of Abbreviations

ABC	Aircraft-Body Centered
AURORA	Autonomous Unmaned Remote Monitoring Robotic Airship

CTI	Center of Information Technology *Renato Archer*
CV	Center of volume
DOA	Degree of Actuation
DoD	United States Department of Defense
DOF	Degrees of Freedom
DRONI	Robotic Airship of Innovative Conception
ECI	Earth-centered inertial
FEM	Faculty of Mechanical Engineering
GMTI	Ground Moving Target Indicator
HAV	Hybrid Air Vehicles
HTA	Heavier-Than-Air
IDSM	Sustainable Development Institute of *Mamirauá*
INDI	Incremental Nonlinear Dynamic Inversion
InSAC	Instituto Nacional de Ciência e Tecnologia para Sistemas Autônomos Cooperativos
IST	Superior Institute of Lisbon
ITA	Air Force Institute of Technology
LEMV	Long Endurance Multi-intelligence Vehicle Project
LTA	Lighter-Than-Air
LTI	Linear Time-Invariant
LTP	Local Tangent Plane
MTI	Moving Target Indicator
NED	North, East, Down
SAS-ROGE	Smart Airships Swarm and Robotic Ground Electrical Vehicles for Environmental Monitoring and Surveillance
SBAI	Brazilian Symposium on Intelligent Automation
SFKC	State Feedback Controller
SMC	Sliding Mode Control
UAV	Unmanned Aerial Vehicle
UFAM	Federal University of *Amazonas*

UNICAMP	University of *Campinas*
VMTI	Visual Moving Target Indicator
VSS	Variable Structure Systems

Contents

1 INTRODUCTION

Over the last years, there has been great scientific and technological advances in hardware, software, and control techniques on mobile robotics, which attracted interest from researchers, engineers, and companies all over the world, both in civilian and military applications. A significant part was focused on Autonomous Terrestrial Vehicles and Heavier-Than-Air (HTA) aerial vehicles, while very little was done for Lighter-Than-Air (LTA) aerial vehicles, such as the AURORA airship (Figure 1.1), which are the focus of this dissertation.

Figure 1.1 Test flight of the AURORA airship (Moutinho (2007))

Regarding Unmanned Aerial Vehicles (UAVs), distinct types of aircrafts (fixed wing, rotorcraft, LTA) have distinct features and perform differently on various applications, which determines the best use for each one. As airships work in low airspeed, they are particularly interesting for low-altitude monitoring missions. Besides, due to its aerostatic lift, airships have very low power consumption as they do not spend energy to maintain themselves afloat. Figure 1.2 illustrates a comparison between different means of transportation, with respect to speed and energy consumption.

Therefore, an operation that could benefit from this type of vehicle would be monitoring atmospheric gases, for example. Currently, the most practical way to make these measurements, on a regional scale, is to use small commercial airplanes, which are costly and limits its frequency.

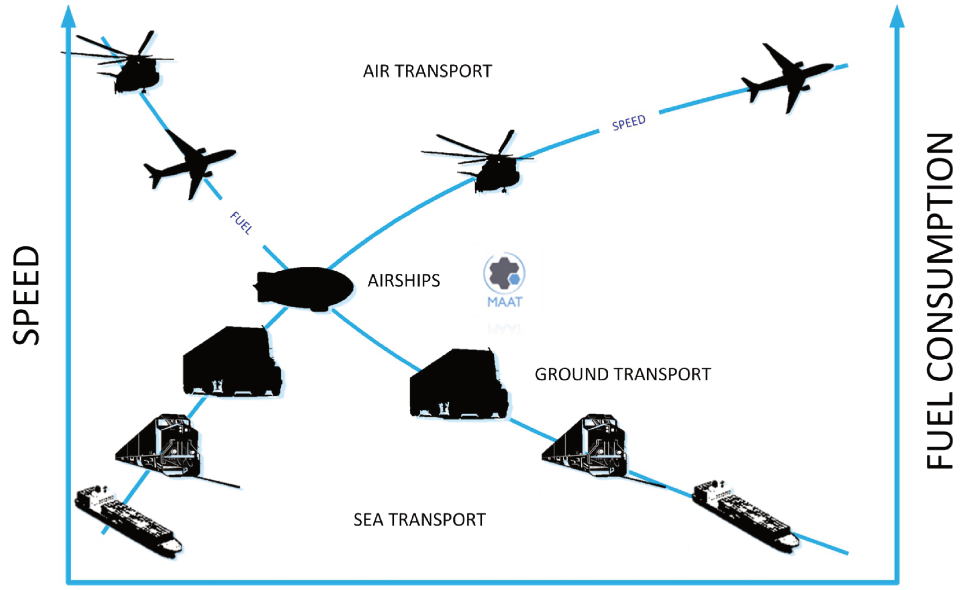

Figure 1.2 Speed and Energy Consumption comparison between different means of transportation (Smith *et al.* (2013))

Employing LTA observation platforms, for environmental applications, shows many advantages over other types of UAVs, as they allow for less power consumption, long observation duration (long endurance mission) and low degree of intrusion in the environment with less noise generation and wind perturbation (Bueno *et al.* (2002)).

Airships have two main applications, presently. The first application involves small autonomous airships, for surveillance and/or monitoring. The second employs large airships, for transport or telecommunication. For the former, there is great strategic interest in high-altitude aircrafts, which could serve as an alternative to satellites in monitoring large areas, or relaying and amplifying communication signals (Colozza e Dolce (2003)). In the year of 2010, in the US, there has been a contest for the Long Endurance Multi-intelligence Vehicle Project (LEMV) from the DoD (US Army (2010)). Among the competitors there was the P-791 from Lockheed Martin (Figure 1.3a) and the HAV 304 from Hybrid Air Vehicles (HAV), which later became Airlander 10 (Figure 1.3b). Both companies developed hybrid airships and HAV 304 was chosen for LEMV project, but it was canceled in 2013. The main difference between a common airship and a hybrid airship is that the latter is not a true LTA, needing aerodynamic lift to maintain itself in the air.

All these scientific and technological advances, in the last 15 years, emphasizes that it is a timely moment to get involved with research around LTA vehicles. Moreover, as it is incipient, there is a chance for Brazil not to become outdated when compared to other countries, as it has happened with terrestrial and HTA vehicles.

(a) The hybrid airship P-791 from Lockheed Martin (b) HAV 304/Airlander 10 from Hybrid Air Vehicles

Figure 1.3 Main competitors for LEMV project, from DoD (US Army (2010))

In this context, the Brazilian pioneering Autonomous Unmaned Remote Monitoring Robotic Airship (AURORA) project (1997-2017) represented a big effort towards this challenge. The over 60 publications of this collaborative Brazil-Portugal development are a reference for researchers and engineers all over the world. Started in 1997 by the Center of Information Technology *Renato Archer* (CTI), this project had the objective of developing technologies and prospection for the increasing autonomy of unmanned airships, for environmental and control monitoring (de Paiva *et al.* (2006)).

During these 20 years of international cooperative research between Brazil-Portugal-France, many cooperation projects were carried out, resulting in important scientific and technological landmarks such as: a complete mathematical model/simulation of the dynamics of airships (Gomes e Ramos (1998); Azinheira *et al.* (2001, 2002); de Paiva *et al.* (2006)); elaborated control system and trajectory tracking for airships in simple cruise flight, whose experimental validation led to the first publication in the world literature, reporting an automated outdoor airship flight (Ramos *et al.* (2001); de Paiva *et al.* (2006)); development of robust nonlinear control and trajectory tracking approaches for a complete flight mission (vertical takeoff/landing, hovering and trajectory tracking) like Feedback Linearization (Moutinho (2007)), Backstepping (Azinheira *et al.* (2009)), Sliding Modes (de Paiva *et al.* (2007); Benjovengo *et al.* (2009); Vieira *et al.* (2017)), Gain Scheduling (Moutinho *et al.* (2016)), and Incremental Nonlinear Dynamic Inversion (INDI) (Azinheira *et al.* (2015)).

The present research work introduces an innovation for the autonomous airships of this research team, as this result is the first attempt of developing guidance and control strategies for multiple cooperative airships in the same environment, executing controlled and coordinated flight.

1.1 Work Context

Recently, in 2014, the seminal AURORA project evolved to a new airship conception, now using a different propulsion configuration (Arias (2014)), incorporating four electrical vectoring thrusters (instead of the classical pair of combustion propellers) to increase the airship maneuverability, especially at low speeds. This is the theme of the DRONI project (CNPq CT-Aeronáutico 2014-2017), also conducted by CTI - *Renato Archer* in partnership with the University of *Campinas* (UNICAMP), Superior Institute of Lisbon (IST), Air Force Institute of Technology (ITA), Federal University of *Amazonas* (UFAM) and Sustainable Development Institute of *Mamirauá* (IDSM). The DRONI project has three specific goals: the design and construction of a new conception of unmanned airship, with quadruple electrical actuation, as well as the associated robotic infrastructure and embedded system; the development in modeling, simulation and control of this new type of aircraft (Arias (2014); Marton (2016)); the execution of pilot-scale application of this robotic airship in the socio-economic and environmental context of the Amazon (Carvalho *et al.* (2014); Pinagé *et al.* (2013)).

Furthermore, it was in the context of the DRONI project that a joint cooperative research Brazil-Scotland was proposed in 2016 under the so-called Smart Airships Swarm and Robotic Ground Electrical Vehicles for Environmental Monitoring and Surveillance (SAS-ROGE) project, between UNICAMP and Heriot-Watt University of Edinburgh (Fapesp Sprint 2016/50001-1). The objective of this project was to develop an Intelligent approach for the control of a swarm of airships. This masters dissertation is related to this project and aims the development, in simulation, of a linear (classical) control strategy that allows for one airship to follow another in the presence of wind and turbulence. The first airship should use a previously established control strategy to follow a predefined path, while the second follows the first and the third can follow the first, or the second (Figure 1.4).

Finally, in the same research line of the DRONI project, the research team joined, in 2016, the Thematic Project Fapesp-CNPq "Instituto Nacional de Ciência e Tecnologia para Sistemas Autônomos Cooperativos (InSAC) in Applied Cooperative Autonomous Systems", more specifically within the working group "lighter-than-air platforms for sensing, communication and information systems applied to the Amazon region", led by CTI - *Renato Archer*, Faculty of Mechanical Engineering (FEM)-UNICAMP, ITA and UFAM. The nonlinear control approaches

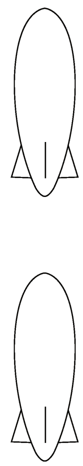

Figure 1.4 Convoy of two airships in column formation

developed in this context by the Portuguese partners, Dr. José Azinheira and Dr. Alexandra Moutinho (IST), in cooperation with Dr. Ely Paiva (UNICAMP) and Dr. José Reginaldo Carvalho (UFAM) will integrate the airship automatic pilot system of the DRONI project to achieve the challenging goals by 2018, when flight experiments will take place in Amazon. The main applications of this work are focused on monitoring and surveillance in the Amazon region, through the existing partnership between UNICAMP/CTI and Prof. Reginaldo Carvalho (UFAM) and the Mamirauá Institute (IDSM), which intends to use cooperative flight to track ground targets, such as wild animals with electronic trackers (on land or rivers), intrusive people or vehicles, movements of vessels, among others (Carvalho *et al.* (2014); Pinagé *et al.* (2013))

This work is focused in the development and simulation of a flight control system, for the coordinated flight of three airships, tracking a moving ground target and it is inserted in the context of four funded projects that are AURORA, DRONI, SAS-ROGE and InSAC.

1.2 Motivation and State of the Art

The coordinated flight of UAVs constitutes an important research area due to the ability to simultaneously cover large areas, increased robustness and performance in the face of failures and efficient cooperation to achieve a common goal (Tsourdos *et al.* (2010)). Surveillance and subsequent tracking of moving targets, whether animals, people or land vehicles, has become one of the most active themes of recent research on cooperative air vehicles (Oh (2013)), which is the main problem addressed in this masters research. In the present context, surveillance means the monitoring of behavior, activities, or other dynamic information, usually of people, animals, or vehicles for influencing, managing, directing, or protecting (Tsourdos *et al.* (2010)).

Aerial surveillance is based on the collection of information, usually from visual images or from another sensorial source positioned in the air vehicle. In the surveillance and monitoring application, involving the search and tracking of mobile ground target, two fields of research in cooperative robotics are particularly important: area coverage and target tracking, which are often performed simultaneously (Pimenta *et al.* (2009)). Area coverage usually involves the use of path planning algorithms to efficiently scan the largest possible area, maximizing the probability of detecting the target object, while tracking involves the detection and tracking of the target in real time. Obviously, both subtasks can be performed more efficiently with the use of multiple UAVs. As the number of UAVs increases, so does their spread and, subsequently, their area of coverage. Moreover, as the quantity of information escalate, so does the robustness of the tracking. In this way, the challenge is the cooperation and coordination of activities between these aircrafts.

Hierarchically, the level of cooperation in each coordinated flight of UAVs can be classified in three separate ways (Oh (2013)). It can be defined by a "command center" in a ground station, for example, where it is called centralized; it can be assigned to aircraft individually, when it is called decentralized; or it can be semi-decentralized when only the "leading" aircraft receives external commands, the rest being distributed autonomously in relation to their closest "companions". In any case, coordinated flight is always a complex task, since it must be planned in relation to the other members of the group, as to avoid collision between aircraft, as well as obstacles (fixed or mobile) in the environment, in addition to the inherent uncertainties.

A typical hierarchy of communication and coordination of mission planning that can be used for the surveillance task, with area coverage and tracking is shown in Figure 1.5 (Tsourdos *et al.* (2010)). This three-tier structure may be defined in a central scheduler or in each UAV, depending on the type of architecture autonomy (centralized or decentralized). The top layer defines and maintains mission objectives, while delegating tasks and allocating resources. The middle layer generates the path planning for the UAVs, considering algorithms to avoid collisions, producing feasible and safe routes for the aircraft, a crucial component in such an autonomous system. The lower layer produces the control actions that ensure that the UAVs will execute the controlled trajectories.

Currently, there are several UAV trajectory planning solutions available in the literature (Shanmugavel (2007); Oh (2013)), depending on the specific application desired, but in general it is possible to present a typical path planner strategy as the sub-block detailed to the right in

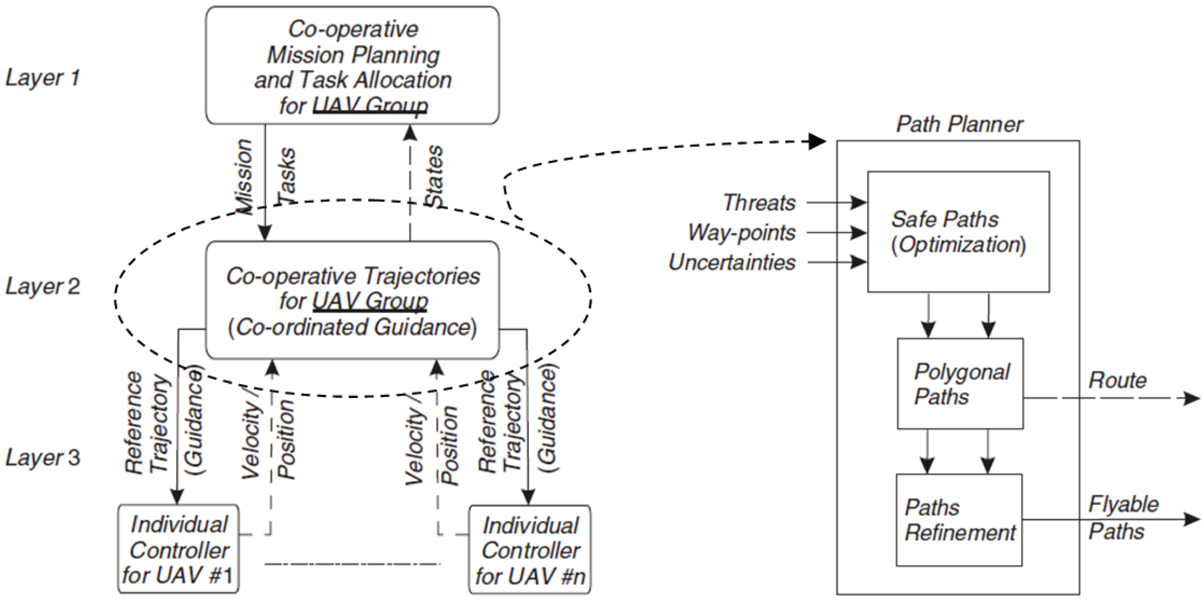

Figure 1.5 Typical hierarchy of mission planning in coordinated flight (left) and detailing a typical trajectory planning structure (right) (Tsourdos *et al.* (2010)).

Figure 1.5 (Tsourdos *et al.* (2010)).

The trajectory planner receives information on the waypoints to be visited, the position and size of obstacles, or prohibited flight areas, and the associated uncertainties. Next, optimization techniques are applied to this data to produce feasible routes, usually defined by straight line segments or polygons. These route optimization methods, however, do not consider the vehicle's kinematic constraints, such as the impossibility to reverse or the minimum radius of curvature that can be executed during a turn. This is the objective of the last stage of the planner sub-block that performs a trajectory refinement. For this, clothoids and splines are used for interpolation between points, but the most common method is to approach the trajectory using only straight lines and circle arcs, as in the well-known Dubins path method (Tsourdos *et al.* (2010)).

The problem of formation flight control for UAVs has already been extensively researched for various aircraft types (Flint *et al.* (2002); Shanmugavel (2007); Oh (2013)), but to the best of the author's knowledge, there is only one work in the literature focused on outdoor airships, which is presented in Bicho *et al.* (2006). In this "leader-follower" approach, the authors propose a control architecture for two airships at a time, which may be column, line or oblique. The distance and orientation between the two airships is controlled keeping the orientation and relative speed between both. This structure is then combined to generate more complex formations such as the known "V" formation, shown in Figure 1.6 and used in this masters work.

The Bicho *et al.* (2006) work, however, does not focus on estimation or target tracking. Other cooperative flight researches of small indoor airships are found in King *et al.* (2004) and Olsen

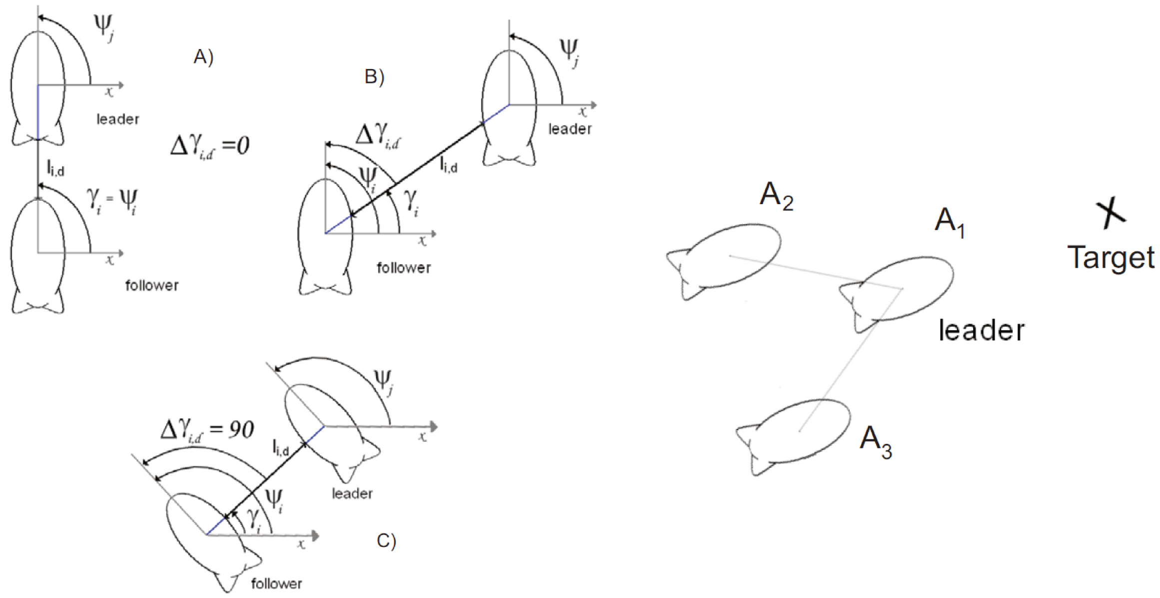

Figure 1.6 Illustration of the flight types in formation of “leader-follower” (Bicho *et al.* (2006)).

et al. (1999). In this case, the task is much easier due to the absence of wind disturbances and turbulence.

In addition to the task of area coverage by the air vehicle, another very important task in this type of application is the surveillance function that is related to the detection and tracking of targets on the ground. Normally, the targets are classified in two types: fixed or mobile. As examples of fixed targets, it is possible to follow the course of a river, a vegetation area, or a topography. As examples of mobile targets, there is the tracking of animals, people, or land vehicles, which is a much more complex situation than the first case, due to the unforeseen maneuvers of the target, as well as the kinematic constraints of the aircraft.

For the case of the moving target, the path planning block of Figure 1.5 assumes different function, from what is shown there, as instead of generating a trajectory, it only provides the desired orientation and speed for the various aircrafts, or for the leading aircraft, in the case of semi-decentralized tracking. The exception is if the moving target moves over a road or over a river, then an approximate path, usually based on maps, may be generated.

In addition to an effective communication system, a UAV tracking system also requires efficient acquisition and target detection techniques. For example, UAVs with a sensory image acquisition or radar system can provide a Moving Target Indicator (MTI) that provides a fast and consistent estimate of many moving targets in soil, Visual Moving Target Indicator (VMTI), or Ground Moving Target Indicator (GMTI) (Oh (2013)). The information obtained from position and velocity of the target can then be used for coordinated control of three or more airships, by pursuing the object cooperatively. There are two typical types of coordinated flights for tracking, much used in the literature. In the first one, the set of UAVs maintains a certain distance from the target (standoff distance), while orbiting it at a given altitude (Oh (2013)), to track it without being noticed, as shown in Figure 1.7, which at the end causes a helical-like displacement of the UAVs.

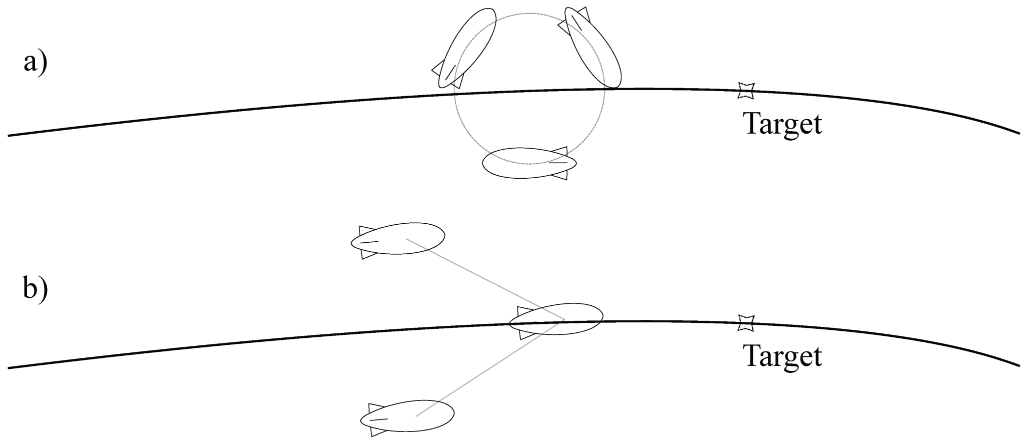

Figure 1.7 Possibilities for the execution of the control of cooperative target tracking in soil.

Another possibility, addressed in this work, is to follow the target at a certain distance using the "leader-follower" diagonal formation flight, also illustrated in Figure 1.7. In both cases, it is intended to obtain a greater precision of the target estimation, taking advantage of the redundancy of the sensors in a sensorial fusion, as well increasing the robustness of the tracking system, in case of failures or occlusion of an individual sensor of a UAV. It should be noted that several tracking approaches have already been proposed and tested for conventional aircraft (airplanes, helicopters, and drones), although not for the coordinated flight of airships, again, to the best of the author's knowledge. The main challenges in this case are the slow dynamics of airships, the underactuation (due to the low lateral controllability) and the strong wind perturbations and turbulence that can represent more than 50% of the current airship airspeed.

1.3 Objectives

The overall objective of this work is the development, testing, and validation in simulated environment, of a flight control system in formation of three airships for the tracking of mobile targets in soil and path following. Therefore, the specific objectives to be achieved in this work plan are:

1. Adaptation of the DRONI dynamical airship simulator (Arias (2014)) for a simulator of the kinematic model, with wind and turbulence.

2. Implementation in the simulator of trajectory planning techniques and kinematic control, for multiple airships, for waypoint navigation and hovering.

3. Development of flight control algorithms in formation of three airships chasing a ground target, in diagonal formation ("V"), using a dynamical airship simulator.

The first objective might seem like a waste at first, since the kinematic implementation is expected to have several issues if not properly adapted to the dynamical case and the core of this work will happen in the dynamical simulator, which is the closest representation of the DRONI airship currently available. However, the dynamical simulator has a plethora of variables and a complexity far greater than the kinematic simulator is expected to have. When multiplying the number of airships the simulator already has, this could lead to an overwhelming number of issues that would greatly slow down the progress of this work. The first step then comes as a minor effort that will help build the foundation for this master's work during the second step. Nevertheless, the last step is expected to take the most development time, due to its natural complexity. It is also the core of this work, so the most effort will have to be put there.

2 AIRSHIP MODELING

This chapter provides the necessary tools for implementing a simulator and control law for the DRONI project airship. The model presented here was developed based on the AURORA project (Moutinho (2007)), predecessor to it, which used two combustion engines instead of the four electric motors that are now used. The simulator of the AURORA project has already been experimentally validated by de Paiva *et al.* (2006).

When working with land vehicles, one quickly learns that control systems are designed according to traction and steering configuration factors (different wheel arrays, treadmills and so on) and the Degree of Actuation (DOA) which ranges from underactuated to holonomic (Morin e Samson (2008)) and that remains true for aircrafts. Therefore it is to be expected that, in spite of the almost non-existent kinematic difference between the two projects, the set of actuators will require a control law different from the one developed by de Paiva *et al.* (2010).

2.1 Kinematic model

The airship modeling begins with the simplest model, which is the kinematic. This applies mainly when speeds are low and other conditions remain close to ideal. The Degrees of Freedom (DOF) will be represented by quaternions ($\mathbf{q} = [q_0\ q_1\ q_2\ q_3]^{\mathrm{T}}$), since the Euler angles ($\mathbf{\Phi} = [\varphi\ \theta\ \psi]^{\mathrm{T}}$) allows Gimbal lock, when one of the DOF is lost by aligning two of the three Euler angles. Such singularity is avoided with quaternions (Titterton e Weston (2004)).

At this point, it is important to note that the airship kinematic model makes use of two, out of four, reference frames. For this work, it suffices to say that the frames are:

- Earth-centered inertial (ECI) - centered at the center of mass of the Earth;
- NED - or Local Tangent Plane (LTP) centered at the surface of the Earth;
- Aircraft-Body Centered (ABC) - centered at the Center of volume (CV) of the airship (Figure 2.1);
- Aerodynamic frame - derived from ABC, considering the aerodynamic incidence angles.

Let there be a ABC linear velocity vector, $\mathbf{v} = [u\ v\ w]^{\mathrm{T}}$ and an angular speed vector, $\boldsymbol{\omega} = [p\ q\ r]^{\mathrm{T}}$. A positioning vector $\boldsymbol{\eta} = [\mathbf{p}^{\mathrm{T}}, \mathbf{q}^{\mathrm{T}}]^{\mathrm{T}} = [p_N\ p_E\ p_D\ q_0\ q_1\ q_2\ q_3]^{\mathrm{T}}$, with respect to the NED frame, can be defined as:

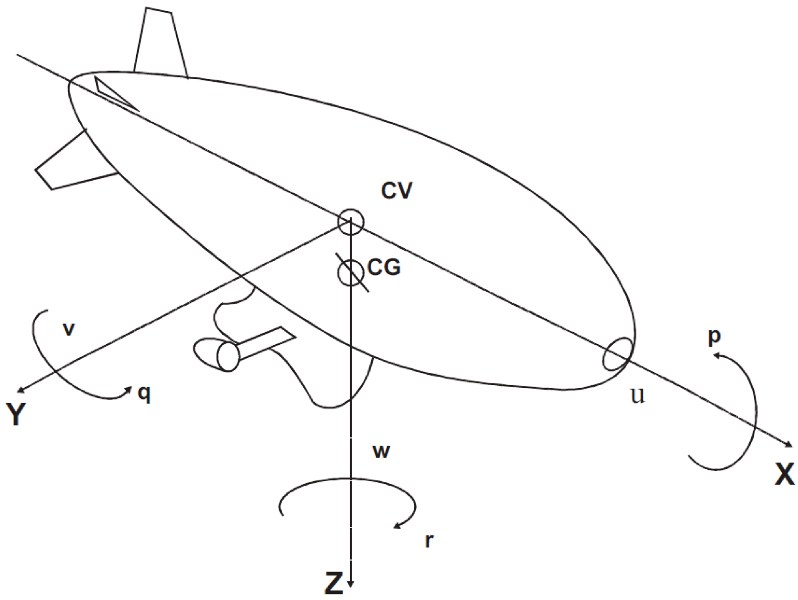

Figure 2.1 Fixed reference frame of the airship (Khoury (2012)).

$$\begin{cases} \dot{\mathbf{p}} = \mathbf{S}^{\mathrm{T}}\mathbf{v} & (2.1) \\ \dot{\mathbf{q}} = \dfrac{1}{2}\mathbf{Q}\begin{bmatrix} 0 \\ \boldsymbol{\omega} \end{bmatrix} & (2.2) \end{cases}$$

$$\dot{\boldsymbol{\eta}} = \begin{bmatrix} \dot{\mathbf{p}} \\ \dot{\mathbf{q}} \end{bmatrix} = \begin{bmatrix} \mathbf{S}^{\mathrm{T}} & 0 \\ 0 & \frac{1}{2}\mathbf{Q} \end{bmatrix} \mathbf{Cx} = \mathbf{DCx} = \mathbf{Tx} \tag{2.3}$$

where

$$\mathbf{Q} = \begin{bmatrix} q_0 & -q_1 & -q_2 & -q_3 \\ q_1 & q_0 & -q_3 & q_2 \\ q_2 & q_3 & q_0 & -q_1 \\ q_3 & -q_2 & q_1 & q_0 \end{bmatrix} \in \mathbb{R}^{4\times 4} \tag{2.4}$$

is the unitary matrix that relates the system angular velocities to quaternions derivatives and $\mathbf{S} \in \mathbb{R}^{3\times 3}$ is the orthogonal transformation matrix, defined by

$$\mathbf{S} = \begin{bmatrix} \cos\psi\cos\theta & \sin\psi\cos\theta & -\sin\theta \\ \cos\psi\sin\theta\sin\varphi - \sin\psi\cos\varphi & \sin\psi\sin\theta\sin\varphi + \cos\psi\cos\varphi & \cos\theta\sin\varphi \\ \cos\psi\sin\theta\cos\varphi + \sin\psi\sin\varphi & \sin\psi\sin\theta\cos\varphi - \cos\psi\sin\varphi & \cos\theta\cos\varphi \end{bmatrix} \in \mathbb{R}^{3\times 3} \tag{2.5}$$

Moreover, $\mathbf{C} = \begin{bmatrix} I_3 & 0_3 \\ 0_{1,3} & 0_{1,3} \\ 0_3 & I_3 \end{bmatrix} \in \mathrm{I\!R}^{7\times 6}$, $\mathbf{D} = \begin{bmatrix} \mathbf{S}^{\mathrm{T}} & 0 \\ 0 & \frac{1}{2}\mathbf{Q} \end{bmatrix} \in \mathrm{I\!R}^{7\times 7}$, $\mathbf{T} = \mathbf{DC} \in \mathrm{I\!R}^{7\times 6}$ and $\mathbf{x} = [\mathbf{v}^{\mathrm{T}}\ \boldsymbol{\omega}^{\mathrm{T}}]^{\mathrm{T}}$ the velocity vector.

The derivatives of the matrices in $\mathbf{D}$ are:

$$\dot{\mathbf{S}} = -\boldsymbol{\Omega}_3 \mathbf{S} \Rightarrow \dot{\mathbf{S}}^{\mathrm{T}} = \mathbf{S}^{\mathrm{T}} \boldsymbol{\Omega}_3 \tag{2.6}$$

and

$$\dot{\mathbf{Q}} = \frac{1}{2} \mathbf{Q} \boldsymbol{\Omega}_4 \tag{2.7}$$

being

$$\boldsymbol{\Omega}_3 = \begin{bmatrix} 0 & -\omega_3 & \omega_2 \\ \omega_3 & 0 & -\omega_1 \\ -\omega_2 & \omega_1 & 0 \end{bmatrix} \tag{2.8}$$

the cross-product matrix equivalent to $\boldsymbol{\omega}\times$ and

$$\boldsymbol{\Omega}_4 = \begin{bmatrix} 0 & -\omega_1 & -\omega_2 & -\omega_3 \\ \omega_1 & 0 & -\omega_3 & \omega_2 \\ \omega_2 & \omega_3 & 0 & -\omega_1 \\ \omega_3 & -\omega_2 & \omega_1 & 0 \end{bmatrix} \tag{2.9}$$

the antisymmetric matrix associated by the angular velocity $\boldsymbol{\omega} = [\omega_1\ \omega_2\ \omega_3]^{\mathrm{T}}$. Thus

$$\dot{\mathbf{D}} = \begin{bmatrix} \mathbf{S}^{\mathrm{T}} \boldsymbol{\Omega}_3 & 0 \\ 0 & \frac{1}{4} \mathbf{Q} \boldsymbol{\Omega}_4 \end{bmatrix} = \begin{bmatrix} \mathbf{S}^{\mathrm{T}} & 0 \\ 0 & \frac{1}{2}\mathbf{Q} \end{bmatrix} \begin{bmatrix} \boldsymbol{\Omega}_3 & 0 \\ 0 & \frac{1}{2}\boldsymbol{\Omega}_4 \end{bmatrix} = \mathbf{D} \boldsymbol{\Omega}_7 \tag{2.10}$$

which will be an important result further on.

It is also possible to define the positioning vector of the airship considering the airspeed ($\mathbf{v}_a$) and a translation constant wind, which yields $\boldsymbol{\eta} = [\mathbf{p}^{\mathrm{T}},\ \mathbf{q}^{\mathrm{T}}]^{\mathrm{T}} \in \mathrm{I\!R}^7$, as composed of Cartesian coordinates $\mathbf{p} \in \mathrm{I\!R}^3$ in the NED geographical coordinate system and angular attitude in quaternions $\mathbf{q} \in \mathrm{I\!R}^4$ (Stevens *et al.* (2015)). The kinematics involves the transformation between position and velocity. The derivative of the position is related to the relative velocity of the airship, given by:

$$\dot{\boldsymbol{\eta}} = \begin{bmatrix} \dot{\mathbf{p}} \\ \dot{\mathbf{q}} \end{bmatrix} = \begin{bmatrix} \mathbf{S}^{\mathrm{T}} & 0 \\ 0 & \frac{1}{2}\mathbf{Q} \end{bmatrix} \mathbf{C} \begin{bmatrix} \mathbf{v} \\ \boldsymbol{\omega} \end{bmatrix} = \begin{bmatrix} \mathbf{S}^{\mathrm{T}} & 0 \\ 0 & \frac{1}{2}\mathbf{Q} \end{bmatrix} \mathbf{C} \begin{bmatrix} \mathbf{v}_a + \mathbf{S}\dot{\mathbf{p}}_w \\ \boldsymbol{\omega} \end{bmatrix} \tag{2.11}$$

$$\dot{\boldsymbol{\eta}} = \begin{bmatrix} \mathbf{S}^{\mathrm{T}} & 0 \\ 0 & \frac{1}{2}\mathbf{Q} \end{bmatrix} \mathbf{C} \begin{bmatrix} \mathbf{v}_a \\ \boldsymbol{\omega} \end{bmatrix} + \begin{bmatrix} I_3 \\ 0_{4\times 3} \end{bmatrix} \dot{\mathbf{p}}_w \tag{2.12}$$

with $\dot{\mathbf{p}}_w = [\dot{p}_{N_w}\ \dot{p}_{E_w}\ \dot{p}_{D_w}]^{\mathrm{T}}$ being the velocity of the air.

Equation 2.11 can be rewritten as:

$$\dot{\boldsymbol{\eta}} = \mathbf{DCx} + \mathbf{B}\dot{\mathbf{p}}_w = \mathbf{Tx} + \mathbf{B}\dot{\mathbf{p}}_w \tag{2.13}$$

where $\mathbf{B} = \begin{bmatrix} I_3 \\ 0_{4\times 3} \end{bmatrix} \in \mathbb{R}^{7\times 4}$.

2.2 Dynamical model - no aerodynamic forces

The kinematics, however, may not be enough to describe the system with the desired precision being necessary to resort to more complex models. The next step is to define a dynamical modeling (Gomes e Ramos (1998); Azinheira *et al.* (2002)) and find a dynamic equation in the form

$$\mathcal{M}\dot{\mathbf{x}} = \mathcal{F}_k + \mathcal{F}_w + \mathcal{F}_g + \mathcal{F}_p \tag{2.14}$$

where $\mathcal{M}$ is the generalized mass matrix and $\mathcal{F}_k$, $\mathcal{F}_w$, $\mathcal{F}_g$ and $\mathcal{F}_p$ are the kinematics, wind, gravity and propulsion generalized force vectors, respectively. For that to happen, some assumptions have to be made first.

1. Given the density of the airship being very close to the air, not only buoyancy is a very significant effect, but the mass and inertia of this air also. This means that the airship will change its dynamics according to the displacement of air around it, as if its mass and inertia were larger than that of its body.

2. Considering the first assumption, three sets of masses are considered to simplify the air displacement effects: the mass and inertia of the airship ($m,\ \mathbf{J}$); the mass and inertia of the displaced air ($m_B,\ \mathbf{J}_B$); the virtual mass and inertia ($\mathbf{M}_v,\ \mathbf{J}_v$), which may be regarded as the kinetic energy of the air displaced by the airship due to its airspeed, this notion was

introduced by Lamb (1918).

3. Despite the change of mass of the airship due to inflation and deflation of the ballonet, its time derivative will be considered zero, since it varies slowly.

4. The airship is a rigid body and aeroelastic effects are neglected.

As the complete modeling of the airship is rather extensive, only the beginning and some key elements will be presented here. The full modeling can be found in Gomes e Ramos (1998), Azinheira *et al.* (2002), Azinheira *et al.* (2006), Moutinho (2007) and de Paiva *et al.* (2008), though Moutinho (2007) is very complete.

With the necessity to account for the air mass displaced by the airship, it is simpler to utilize a Lagrangian approach, rather than that of Newton. The total kinetic energy (W) is obtained through the sum (Azinheira *et al.* (2002))

$$W = W^c + W_B + W_v \tag{2.15}$$

which is the sum of:

- The kinetic energy of the vehicle itself (W^c), which depends on its inertial velocity and mass. Let $\mathbf{x}^c \in \mathbb{R}^{6\times1}$ be the inertial velocity of the airship and $\mathcal{M}^c = \begin{bmatrix} mI_3 & 0 \\ 0 & \mathbf{J}^c \end{bmatrix}$ the generalized mass matrix, both referenced to the center of gravity (CG) (c superscript). Then
$$W^c = \frac{1}{2}\mathbf{x}^{c\mathrm{T}}\mathcal{M}^c\mathbf{x}^c \tag{2.16}$$

- The energy added to the displaced air (W_B). Consider $\mathbf{x}$ the inertial velocity of the airship, $\mathbf{x}_a = \mathbf{x} - \mathbf{x}_w$ the airspeed of the airship and $\mathbf{x}_w$ the wind velocity, the three referenced to the CV (no superscript). $\mathcal{M}_B \in \mathbb{R}^{6\times6}$ is the inertial mass matrix of the buoyancy air. Then
$$W_B = \frac{1}{2}(\mathbf{x}_a{}^{\mathrm{T}}\mathcal{M}_B\mathbf{x}_a - \mathbf{x}^{\mathrm{T}}\mathcal{M}_B\mathbf{x}) \tag{2.17}$$

- The energy due to the virtual mass (W_v). If $\mathcal{M}_v \in \mathbb{R}^{6\times6}$ is the generalized mass matrix of the virtual mass, then
$$W_v = \frac{1}{2}\mathbf{x}_a{}^{\mathrm{T}}\mathcal{M}_v\mathbf{x}_a \tag{2.18}$$

The first term, being the only referenced to the CG, has to be shifted to the CV. Let $\mathbf{c}$ be the vector from the CV to the CG, then

$$\mathbf{v}^c = \mathbf{v} - \mathbf{c} \times \boldsymbol{\omega} \tag{2.19}$$

Knowing that $\boldsymbol{\omega}^c = \boldsymbol{\omega}$, Equation 2.19 leads to

$$\mathbf{x}^c = \begin{bmatrix} \mathbf{I} & -\mathbf{C}_3 \\ 0 & \mathbf{I} \end{bmatrix} \mathbf{x} \tag{2.20}$$

with $\mathbf{C}_3$, as it was with $\boldsymbol{\Omega}_3$, being the cross-product matrix equivalent to $\mathbf{c}\times$. Substituting on Equation 2.16 leads to

$$W^c = \frac{1}{2}\mathbf{x}^{\mathrm{T}} \begin{bmatrix} \mathbf{I} & 0 \\ \mathbf{C}_3 & \mathbf{I} \end{bmatrix} \mathcal{M}^c \begin{bmatrix} \mathbf{I} & -\mathbf{C}_3 \\ 0 & \mathbf{I} \end{bmatrix} \mathbf{x} = \frac{1}{2}\mathbf{x}^{\mathrm{T}}\mathcal{M}\mathbf{x} \tag{2.21}$$

with $\mathcal{M} = \begin{bmatrix} mI_3 & -m\mathbf{C}_3 \\ m\mathbf{C}_3 & \mathbf{J} \end{bmatrix}$ and $\mathbf{J} = \mathbf{J}^c - m\mathbf{C}_3^{\mathrm{T}}\mathbf{C}_3$

Lastly, since the relative velocity $\mathbf{x}_a = \mathbf{x} - \mathbf{x}_w$, the total energy, given by the sum in Equation 2.15 can be expressed as

$$\begin{aligned} W &= W^c + W_B + W_v \\ &= \frac{1}{2}(\mathbf{x}^{\mathrm{T}}\mathcal{M}\mathbf{x} + \mathbf{x}_a{}^{\mathrm{T}}\mathcal{M}_B\mathbf{x}_a - \mathbf{x}^{\mathrm{T}}\mathcal{M}_B\mathbf{x} + \mathbf{x}_a{}^{\mathrm{T}}\mathcal{M}_v\mathbf{x}_a) \\ &= \frac{1}{2}(\mathbf{x}^{\mathrm{T}}(\mathcal{M} - \mathcal{M}_B)\mathbf{x} + (\mathbf{x} - \mathbf{x}_w)^{\mathrm{T}}(\mathcal{M}_B + \mathcal{M}_v)(\mathbf{x} - \mathbf{x}_w)) \\ &= \frac{1}{2}(\mathbf{x}^{\mathrm{T}}(\mathcal{M} + \mathcal{M}_v)\mathbf{x} - 2\mathbf{x}^{\mathrm{T}}(\mathcal{M}_B + \mathcal{M}_v)\mathbf{x}_w + \mathbf{x}_w{}^{\mathrm{T}}(\mathcal{M}_B + \mathcal{M}_v)\mathbf{x}_w) \\ &= \frac{1}{2}(\mathbf{x}^{\mathrm{T}}\mathcal{M}_a\mathbf{x} - 2\mathbf{x}^{\mathrm{T}}\mathcal{M}_{Ba}\mathbf{x}_w + \mathbf{x}_w{}^{\mathrm{T}}\mathcal{M}_{Ba}\mathbf{x}_w) \end{aligned} \tag{2.22}$$

where $\mathcal{M}_a = \mathcal{M} + \mathcal{M}_v = \begin{bmatrix} \mathbf{M}_a & -m\mathbf{C}_3 \\ m\mathbf{C}_3 & \mathbf{J}_a \end{bmatrix}$ and $\mathcal{M}_{Ba} = \mathcal{M}_B + \mathcal{M}_v = \begin{bmatrix} m_B I_3 + \mathbf{M}_v & 0 \\ 0 & \mathbf{J}_B + \mathbf{J}_v \end{bmatrix}$ are symmetric matrices.

Defining a generalized positioning vector $\boldsymbol{\nu} = [\mathbf{p}^{\mathrm{T}}, \boldsymbol{\Phi}^{\mathrm{T}}]^{\mathrm{T}} = [p_N\, p_E\, p_D\, \varphi\, \theta\, \psi]^{\mathrm{T}}$ and its time derivative $\dot{\boldsymbol{\nu}} = \mathbf{G}\mathbf{x}$ (notice that, unlike $\boldsymbol{\eta}$, $\boldsymbol{\nu}$ uses Euler angles), with

$$\mathbf{G} = \begin{bmatrix} \mathbf{S}^{\mathrm{T}} & 0 \\ 0 & \mathbf{R} \end{bmatrix} \tag{2.23}$$

and

$$\mathbf{R} = \begin{bmatrix} 1 & \sin\varphi\tan\theta & \cos\varphi\tan\theta \\ 0 & \cos\varphi & -\sin\varphi \\ 0 & \dfrac{\sin\varphi}{\cos\theta} & \dfrac{\cos\varphi}{\cos\theta} \end{bmatrix} \tag{2.24}$$

the Lagrangian equations of motion may be given by:

$$\mathcal{F}(\dot{\boldsymbol{\nu}}, \boldsymbol{\nu}) = \frac{\mathrm{d}}{\mathrm{d}t}\frac{\partial W}{\partial \dot{\boldsymbol{\nu}}} - \frac{\partial W}{\partial \boldsymbol{\nu}} \tag{2.25}$$

where $W(\dot{\boldsymbol{\nu}}, \boldsymbol{\nu})$ is the system kinetic energy expressed as function of the generalized coordinates $\boldsymbol{\nu}$ and their time derivatives $\dot{\boldsymbol{\nu}}$, and $\mathcal{F}(\dot{\boldsymbol{\nu}}, \boldsymbol{\nu}) = \mathcal{F}_{\boldsymbol{\nu}}$ is the generalized forces vector.

Starting with first term, the proper substitutions result in

$$W_1 = \frac{1}{2}\mathbf{x}^{\mathrm{T}}\mathcal{M}_a\mathbf{x} = \frac{1}{2}\dot{\boldsymbol{\nu}}^{\mathrm{T}}{\mathbf{G}^{-1}}^{\mathrm{T}}\mathcal{M}_a\mathbf{G}^{-1}\dot{\boldsymbol{\nu}} \tag{2.26}$$

which allows for an easy computation of the partial derivative with respect to $\dot{\boldsymbol{\nu}}$,

$$\frac{\partial W_1}{\partial \dot{\boldsymbol{\nu}}} = {\mathbf{G}^{-1}}^{\mathrm{T}}\mathcal{M}_a\mathbf{G}^{-1}\dot{\boldsymbol{\nu}} \tag{2.27}$$

Now, its time derivative can be obtained:

$$\begin{aligned} \frac{\mathrm{d}}{\mathrm{d}t}\frac{\partial W_1}{\partial \dot{\boldsymbol{\nu}}} = {\mathbf{G}^{-1}}^{\mathrm{T}}\mathcal{M}_a\mathbf{G}^{-1}\dot{\boldsymbol{\nu}} &= \frac{\mathrm{d}}{\mathrm{d}t}\left({\mathbf{G}^{-1}}^{\mathrm{T}}\right)\mathcal{M}_a\mathbf{G}^{-1}\dot{\boldsymbol{\nu}} + {\mathbf{G}^{-1}}^{\mathrm{T}}\mathcal{M}_a(\dot{\mathbf{G}^{-1}})\dot{\boldsymbol{\nu}} + {\mathbf{G}^{-1}}^{\mathrm{T}}\mathcal{M}_a\mathbf{G}^{-1}\ddot{\boldsymbol{\nu}} \\ &= \frac{\mathrm{d}}{\mathrm{d}t}\left({\mathbf{G}^{-1}}^{\mathrm{T}}\right)\mathcal{M}_a\mathbf{G}^{-1}\dot{\boldsymbol{\nu}} + {\mathbf{G}^{-1}}^{\mathrm{T}}\mathcal{M}_a((\dot{\mathbf{G}^{-1}})\dot{\boldsymbol{\nu}} + \mathbf{G}^{-1}\ddot{\boldsymbol{\nu}}) \\ &= \frac{\mathrm{d}}{\mathrm{d}t}\left({\mathbf{G}^{-1}}^{\mathrm{T}}\right)\mathcal{M}_a\mathbf{x} + {\mathbf{G}^{-1}}^{\mathrm{T}}\mathcal{M}_a\dot{\mathbf{x}} \end{aligned} \tag{2.28}$$

The partial derivative of the first term, with respect to $\boldsymbol{\nu}$ is:

$$\begin{aligned} \frac{\partial W_1}{\partial \boldsymbol{\nu}} &= \frac{1}{2}\frac{\partial^2}{\partial\boldsymbol{\nu}\partial\dot{\boldsymbol{\nu}}}^{\mathrm{T}}{\mathbf{G}^{-1}}^{\mathrm{T}}\mathcal{M}_a\mathbf{G}^{-1}\dot{\boldsymbol{\nu}} \\ &= \mathbf{K}\mathcal{M}_a\mathbf{x} \end{aligned} \tag{2.29}$$

being

$$\mathbf{K} = \frac{\partial}{\partial\boldsymbol{\nu}}\mathbf{G}^{-1}\dot{\boldsymbol{\nu}} = \begin{bmatrix} \frac{\partial}{\partial\mathbf{p}}\mathbf{G}^{-1}\dot{\boldsymbol{\nu}} \\ \frac{\partial}{\partial\boldsymbol{\Phi}}\mathbf{G}^{-1}\dot{\boldsymbol{\nu}} \end{bmatrix} = \begin{bmatrix} 0 & 0 \\ \mathbf{K}_1 & \mathbf{K}_2 \end{bmatrix}, \quad \mathbf{K}_{1,2} \in \mathbb{R}^{3\times 3} \tag{2.30}$$

Finally, the generalized force, relative to the kinetic energy with no wind, can be obtained in accordance to Equation 2.25:

$$\mathcal{F}_1(\dot{\boldsymbol{\nu}},\boldsymbol{\nu}) = \frac{\mathrm{d}}{\mathrm{d}t}\left(\mathbf{G}^{-1^{\mathrm{T}}}\right)\mathcal{M}_a\mathbf{x} + \mathbf{G}^{-1^{\mathrm{T}}}\mathcal{M}_a\dot{\mathbf{x}} - \mathbf{K}\mathcal{M}_a\mathbf{x} \tag{2.31}$$

The same procedure is applied to the second and third terms, yielding

$$\mathcal{F}_2(\dot{\boldsymbol{\nu}},\boldsymbol{\nu}) = -\mathbf{G}^{-1^{\mathrm{T}}}\mathcal{M}_{Ba}\dot{\mathbf{x}}_w - \frac{\mathrm{d}}{\mathrm{d}t}\left(\mathbf{G}^{-1^{\mathrm{T}}}\right)\mathcal{M}_{Ba}\mathbf{x}_w + \mathbf{K}_w\mathcal{M}_{Ba}\mathbf{x} + \mathbf{K}\mathcal{M}_{Ba}\mathbf{x}_w \tag{2.32}$$

and

$$\mathcal{F}_3(\dot{\boldsymbol{\nu}},\boldsymbol{\nu}) = -\mathbf{K}_w\mathcal{M}_{Ba}\mathbf{x}_w \tag{2.33}$$

and the sum of the three terms is

$$\begin{aligned}\mathcal{F}(\dot{\boldsymbol{\nu}},\boldsymbol{\nu}) =&\mathcal{F}_1(\dot{\boldsymbol{\nu}},\boldsymbol{\nu}) + \mathcal{F}_2(\dot{\boldsymbol{\nu}},\boldsymbol{\nu}) + \mathcal{F}_3(\dot{\boldsymbol{\nu}},\boldsymbol{\nu}) \\ =&\frac{\mathrm{d}}{\mathrm{d}t}\left(\mathbf{G}^{-1^{\mathrm{T}}}\right)\mathcal{M}_a\mathbf{x} + \mathbf{G}^{-1^{\mathrm{T}}}\mathcal{M}_a\dot{\mathbf{x}} - \mathbf{K}\mathcal{M}_a\mathbf{x} - \mathbf{G}^{-1^{\mathrm{T}}}\mathcal{M}_{Ba}\dot{\mathbf{x}}_w \\ &- \frac{\mathrm{d}}{\mathrm{d}t}\left(\mathbf{G}^{-1^{\mathrm{T}}}\right)\mathcal{M}_{Ba}\mathbf{x}_w + \mathbf{K}_w\mathcal{M}_{Ba}\mathbf{x} + \mathbf{K}\mathcal{M}_{Ba}\mathbf{x}_w - \mathbf{K}_w\mathcal{M}_{Ba}\mathbf{x}_w\end{aligned} \tag{2.34}$$

which corresponds to the dynamics of the airship in the local frame. To transform to the inertial frame, the relation $\mathcal{F}_{\mathbf{x}} = \mathbf{G}^{\mathrm{T}}\mathcal{F}_{\boldsymbol{\nu}}$ has to be used. With that, the generalized forces of the airship in the inertial frame is then given by:

$$\begin{aligned}\mathcal{F}(\mathbf{x}) =&\mathcal{M}_a\dot{\mathbf{x}} - \mathcal{M}_{Ba}\dot{\mathbf{x}}_w + \left[\left(\mathbf{G}^{\mathrm{T}}\frac{\mathrm{d}}{\mathrm{d}t}\left(\mathbf{G}^{-1^{\mathrm{T}}}\right) - \mathbf{G}^{\mathrm{T}}\mathbf{K}\right)\mathcal{M}_a + \mathbf{G}^{\mathrm{T}}\mathbf{K}_w\mathcal{M}_{Ba}\right]\mathbf{x} \\ &+ \left(\mathbf{G}^{\mathrm{T}}\mathbf{K} - \mathbf{G}^{\mathrm{T}}\mathbf{K}_w - \mathbf{G}^{\mathrm{T}}\frac{\mathrm{d}}{\mathrm{d}t}\left(\mathbf{G}^{-1^{\mathrm{T}}}\right)\right)\mathcal{M}_{Ba}\mathbf{x}_w\end{aligned} \tag{2.35}$$

Further simplification of Equation 2.35 can be achieved, after considering the following equalities

$$\mathbf{V}_3 = -\mathbf{R}^{\mathrm{T}}\mathbf{K}_1 \tag{2.36}$$

$$\boldsymbol{\Omega}_3 = \mathbf{R}^{\mathrm{T}}\left(\frac{\mathrm{d}}{\mathrm{d}t}\left(\mathbf{R}^{-1^{\mathrm{T}}}\right) - \mathbf{K}_2\right) \tag{2.37}$$

$$\mathbf{V}_{w3} = -\mathbf{R}^{\mathrm{T}}\mathbf{K}_{w1} \tag{2.38}$$

$$0 = \mathbf{R}^{\mathrm{T}}\mathbf{K}_{w2} \tag{2.39}$$

where $\mathbf{V}_3$ and $\mathbf{V}_{w3}$, as is $\boldsymbol{\Omega}_3$, are the cross-product matrix equivalent to $\mathbf{v}\times$ and $\mathbf{v}_w\times$, respectively.

This leads to:

$$\mathbf{G}^{\mathrm{T}} \frac{\mathrm{d}}{\mathrm{d}t}\left(\mathbf{G}^{-1^{\mathrm{T}}}\right) - \mathbf{G}^{\mathrm{T}}\mathbf{K} = \boldsymbol{\Omega}_6 + \mathbf{V}_6 \tag{2.40}$$

$$\mathbf{G}^{\mathrm{T}}\mathbf{K}_w = -\mathbf{V}_{w6} \tag{2.41}$$

with

$$\mathbf{V}_6 = \begin{bmatrix} 0 & 0 \\ \mathbf{V}_3 & 0 \end{bmatrix}, \quad \boldsymbol{\Omega}_6 = \begin{bmatrix} \boldsymbol{\Omega}_3 & 0 \\ 0 & \boldsymbol{\Omega}_3 \end{bmatrix} \text{ and } \quad \mathbf{V}_{w6} = \begin{bmatrix} 0 & 0 \\ \mathbf{V}_{w3} & 0 \end{bmatrix} \tag{2.42}$$

In this way, the dynamics equation of the airship, referenced by the inertial frame, can be represented by:

$$\begin{aligned} \mathcal{F}(\mathbf{x}) =& \mathcal{M}_a\dot{\mathbf{x}} - \mathcal{M}_{Ba}\dot{\mathbf{x}}_w + \left[\left(\boldsymbol{\Omega}_6 + \mathbf{V}_6\right)\mathcal{M}_a - \mathbf{V}_{w6}\mathcal{M}_{Ba}\right]\mathbf{x} \\ &+ \left(\mathbf{V}_{w6} - \boldsymbol{\Omega}_6 - \mathbf{V}_6\right)\mathcal{M}_{Ba}\mathbf{x}_w \end{aligned} \tag{2.43}$$

or, in matrix form:

$$\mathcal{F}(\mathbf{x}) = \begin{bmatrix} \mathcal{M}_a & -\mathcal{M}_{Ba} \end{bmatrix} \dot{\mathbf{X}} + \begin{bmatrix} \boldsymbol{\Omega}_6 + \mathbf{V}_6 & \mathbf{V}_{w6} \end{bmatrix} \begin{bmatrix} \mathcal{M}_a & -\mathcal{M}_{Ba} \\ -\mathcal{M}_{Ba} & \mathcal{M}_{Ba} \end{bmatrix} \mathbf{X} \tag{2.44}$$

in accordance with the equations derived by Thomasson (2000), using quasicoordinates, without the gradient terms.

Analogously, the dynamics equation of the airship in the air frame are also obtainable. The development will be omitted here. The mentioned equation, according to Moutinho (2007) is

$$\mathcal{F}(\mathbf{x}) = \mathcal{M}_a\dot{\mathbf{x}}_a + \boldsymbol{\Omega}_6\mathcal{M}_a\mathbf{x}_a \tag{2.45}$$

discounting for any aerodynamic forces.

Recalling Equation 2.14, taking in consideration the formulations referenced to the local frame, the kinematic ($\mathcal{F}_k$) and wind ($\mathcal{F}_w$) forces are represented by Equation 2.45 ($\mathcal{F}_k + \mathcal{F}_w = \mathcal{F}_{kw} = \mathcal{M}_a\dot{\mathbf{x}}_a + \boldsymbol{\Omega}_6\mathcal{M}_a\mathbf{x}_a$). There is still need to define the propulsion and gravity forces. As the name implies, propulsion forces are the ones generated by the four electric motors, so the acting forces and torques will be represented by $\mathbf{u} = (\mathbf{f}_u, \boldsymbol{\tau}_u)$ and are considered as the system inputs. As for the gravitation force, Azinheira *et al.* (2002) define it in the local frame as:

$$\mathcal{F}_g = \begin{bmatrix} \mathbf{S}(m - m_B)\mathbf{g} \\ \mathbf{C}_3\mathbf{S}m\mathbf{g} \end{bmatrix} = \begin{bmatrix} m_w I_3 \\ m\mathbf{C}_3 \end{bmatrix} \mathbf{Sg} = \mathbf{ESg} \tag{2.46}$$

with $\mathbf{g} = [0\ 0\ g]^{\mathrm{T}}$ being the gravity acceleration, given in the inertial frame and $m_w = m - m_B$ the weighting mass of the airship, which is the difference between its weight and its buoyancy.

Finally, the original airship dynamics, without aerodynamic forces, can be represented by

$$\begin{cases} \mathbf{M}_a\dot{\mathbf{v}} - m\mathbf{C}_3\dot{\boldsymbol{\omega}} = m\boldsymbol{\Omega}_3\mathbf{C}_3\boldsymbol{\omega} - \boldsymbol{\Omega}_3\mathbf{M}_a\mathbf{v} + m_w\mathbf{Sg} + \mathbf{f}_u & (2.47) \\ m\mathbf{C}_3\dot{\mathbf{v}} + \mathbf{J}_a\dot{\boldsymbol{\omega}} = -\boldsymbol{\Omega}_3\mathbf{J}_a\boldsymbol{\omega} - m\boldsymbol{\Omega}_3\mathbf{C}_3\mathbf{v} + m\mathbf{C}_3\mathbf{Sg} + \boldsymbol{\tau}_u & (2.48) \end{cases}$$

in the local coordinate system.

Alternatively, in matrix form:

$$\begin{bmatrix} \mathbf{M}_a & -m\mathbf{C}_3 \\ m\mathbf{C}_3 & \mathbf{J}_a \end{bmatrix} \begin{bmatrix} \dot{\mathbf{v}} \\ \dot{\boldsymbol{\omega}} \end{bmatrix} = - \begin{bmatrix} \boldsymbol{\Omega}_3 & 0 \\ 0 & \boldsymbol{\Omega}_3 \end{bmatrix} \begin{bmatrix} \mathbf{M}_a & -m\mathbf{C}_3 \\ m\mathbf{C}_3 & \mathbf{J}_a \end{bmatrix} \begin{bmatrix} \mathbf{v} \\ \boldsymbol{\omega} \end{bmatrix} + \begin{bmatrix} m_w I_3 \\ m\mathbf{C}_3 \end{bmatrix} \mathbf{Sg} + \begin{bmatrix} \mathbf{f}_u \\ \boldsymbol{\tau}_u \end{bmatrix} \tag{2.49}$$

or, in a compact notation,

$$\mathcal{M}\dot{\mathbf{x}} = -\boldsymbol{\Omega}_6\mathcal{M}\mathbf{x} + \mathbf{ESg} + \mathbf{u} \tag{2.50}$$

2.3 Dynamical model - complete

In the case of the AURORA airship, it was also necessary to have a more complex model that takes into account the aerodynamic effects on system behavior. Among them, the virtual mass and inertia of the airship, caused by the large amount of displaced air mass (Gomes e Ramos (1998); Azinheira *et al.* (2002)).

$$\mathcal{M} \begin{bmatrix} \dot{\mathbf{v}} \\ \dot{\boldsymbol{\omega}} \end{bmatrix} = \mathcal{F}_d \begin{bmatrix} \mathbf{v} \\ \boldsymbol{\omega} \end{bmatrix} + \mathcal{F}_a \begin{bmatrix} \mathbf{v} \\ \boldsymbol{\omega} \end{bmatrix} + \mathcal{F}_p + \mathcal{F}_w + \mathcal{F}_g \tag{2.51}$$

where $\mathcal{M} \in \mathbb{R}^{6\times6}$ is, again, the mass and generalized inertia matrix and $\mathbf{v} \in \mathbb{R}^3$ and $\boldsymbol{\omega} \in \mathbb{R}^3$ are the vectors of inertial and angular velocities in the local reference frame. The forces present on the right side of the equation are: $\mathcal{F}_d$ - centrifugal forces, pseudo-force of Coriolis and forces induced by the wind (Azinheira *et al.* (2002)); $\mathcal{F}_a$ - aerodynamic forces and moments; $\mathcal{F}_p$ - forces and moments of propulsion; $\mathcal{F}_w$ - forces due to the dynamics of the wind and, finally, $\mathcal{F}_g$

- forces and gravitational moments.

It can be seen that this description of the system only has time-derivative states. A more complete system has twelve states, in addition to $\mathbf{v}$ and $\boldsymbol{\omega}$, there are still the Euler angles ($\boldsymbol{\Phi} = [\varphi\ \theta\ \psi]^{\mathrm{T}}$) and the Cartesian positions of the CV in the NED system ($\mathbf{p} = [P_N\ P_E\ P_D]^{\mathrm{T}}$). Thus, the dynamical states $\mathbf{x}$ of an airship can be described as

$$\mathbf{x} = [\mathbf{v}^{\mathrm{T}}\ \boldsymbol{\omega}^{\mathrm{T}}\ \boldsymbol{\Phi}^{\mathrm{T}}\ \mathbf{p}^{\mathrm{T}}]^{\mathrm{T}} = [u\ v\ w\ p\ q\ r\ \varphi\ \theta\ \psi\ P_N\ P_E\ P_D]^{\mathrm{T}} \tag{2.52}$$

As previously mentioned, the DRONI airship has four electric motors, which makes the modeling of its actuators different from what was used in the AURORA project (de Paiva *et al.* (2006)). The airship actuators are shown in Figure 2.2

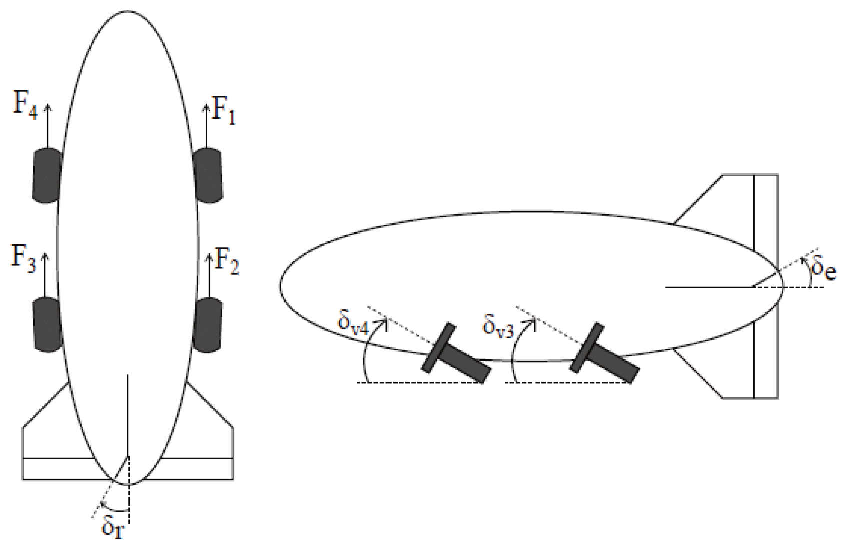

Figure 2.2 DRONI airship actuators representation (Marton (2016)). This airship presents four electric motors with independent intensity and vectorization actuation. It also presents both elevator and rudder wings on the back.

As it can be noticed, there is an intensity ($F_i,\ i \in \{1, \dots, 4\}$) and angular ($\delta_{vi}$) control of the motors in addition to the rudder (δ_r) and elevator (δ_e) deflection. The intensity control is made by the current control input (δ_i) sent to the motors. With this, the input vector $\mathbf{u}$ of the airship is

$$\mathbf{u} = [\delta_e\ \delta_r\ \delta_1\ \delta_2\ \delta_3\ \delta_4\ \delta_{v1}\ \delta_{v2}\ \delta_{v3}\ \delta_{v4}]^{\mathrm{T}} \tag{2.53}$$

However, it is not interesting to manipulate these ten control inputs individually. Instead, the model is separated into longitudinal and lateral dynamics and new control parameters are defined. In the longitudinal model there is $\mathbf{u}_{long} = [\delta_e\ \delta_{tt}\ \delta_{fb}\ \delta_{tv}]^{\mathrm{T}}$ and in the lateral, $\mathbf{u}_{lat} = [\delta_r\ \delta_{cd}]^{\mathrm{T}}$, these being:

- δ_e Elevator deflection angle;
- δ_{tt} Total thrust, summed in all δ_i;
- δ_{fb} Differential thrust Front-Back. Summed from $\delta_{1,4}$ and subtracted from $\delta_{2,3}$;
- δ_{tv} Thrust Vectoring. Equal to all δ_{vi};
- δ_r Rudder deflection angle;
- δ_{cd} Cross differential thrust. Summed from $\delta_{1,3}$ and subtracted from $\delta_{2,4}$.

2.4 Dynamical model - linearized

As explained in the work of Moutinho (2007), the complexity of the nonlinear dynamic equations are impeditive for the design of control laws. The solution is to obtain, through linearization, a Linear Time-Invariant (LTI) system of the form:

$$\dot{x} = Ax + Bu \tag{2.54}$$

This section describes the linearization done by Moutinho (2007) and adapted for the DRONI airship by Marton (2016).

The standard procedure to linearize a model is to utilize the Taylor series expansion around an equilibrium point (x_e, u_e), satisfying $f(x_e, u_e) = 0$. Considering a deterministic model (no disturbances) of the airship, its dynamic equation can be represented by:

$$\dot{x} = f(x, u) \tag{2.55}$$

and the Taylor expansion is

$$\dot{x} \approx f(x_e, u_e) + \left.\frac{\partial f}{\partial x}\right|_{x=x_e, u=u_e} (x - x_e) + \left.\frac{\partial f}{\partial u}\right|_{x=x_e, u=u_e} (u - u_e) \tag{2.56}$$

Substituting the jacobian matrices (A, B)

$$A = \left.\frac{\partial f}{\partial x}\right|_{x=x_e, u=u_e} \tag{2.57}$$

$$B = \left.\frac{\partial f}{\partial u}\right|_{x=x_e, u=u_e} \tag{2.58}$$

and changing variables

$$\tilde{x} = x - x_e \tag{2.59}$$

$$\tilde{u} = u - u_e \tag{2.60}$$

yields:

$$\dot{\tilde{x}} = A\tilde{x} + B\tilde{u} \tag{2.61}$$

As not all terms of the dynamic model are analytical, the differentiation has to be done numerically. This can be accomplished by computing each element of the matrices as

$$A_{ij} = \frac{\partial f_i}{\partial x_j} \approx \frac{f_i(x_e + \Delta x_j, u_e) - f_i(x_e, u_e)}{\Delta x_j} \tag{2.62}$$

$$B_{ij} = \frac{\partial f_i}{\partial x_j} \approx \frac{f_i(x_e, u_e + \Delta u_j) - f_i(x_e, u_e)}{\Delta u_j} \tag{2.63}$$

The A and B matrices vary with the airspeed defined and chosen constraints. The trimming process is detailed in both Moutinho (2007) and Marton (2016).

Lateral model

As previously stated, it is not interesting to manipulate the ten control inputs individually, so the model is decoupled in lateral and longitudinal. This subsection describes the lateral model, which has states

$$\tilde{\mathbf{x}}_{lat} = [\tilde{v}\,\tilde{p}\,\tilde{r}\,\tilde{\varphi}]^{\mathrm{T}} \tag{2.64}$$

and control inputs

$$\tilde{\mathbf{u}}_{lat} = \left[\tilde{\delta}_r\,\tilde{\delta}_{cd}\right]^{\mathrm{T}} \tag{2.65}$$

as described in the end of section 2.3. These state and input vectors lead to the lateral dynamic equation:

$$\begin{bmatrix} \dot{\tilde{v}} \\ \dot{\tilde{p}} \\ \dot{\tilde{r}} \\ \dot{\tilde{\varphi}} \end{bmatrix} = A_{lat} \begin{bmatrix} \tilde{v} \\ \tilde{p} \\ \tilde{r} \\ \tilde{\varphi} \end{bmatrix} + B_{lat} \begin{bmatrix} \tilde{\delta}_r \\ \tilde{\delta}_{cd} \end{bmatrix} \tag{2.66}$$

with matrices A_{lat} and B_{lat} defined by Equation 2.62 and Equation 2.63.

One might question that ψ is not a part of the lateral dynamic equation, that happens because it does not interfere with stability in trimming conditions. However, it can be calculated by the equation:

$$\dot{\tilde{\psi}} = \frac{\tilde{r}}{\cos(\theta_e)} \tag{2.67}$$

Longitudinal model

For the longitudinal model, the dynamic states are

$$\tilde{\mathbf{x}}_{long} = \begin{bmatrix} \tilde{u} \; \tilde{w} \; \tilde{q} \; \tilde{\theta} \end{bmatrix}^{\mathrm{T}} \tag{2.68}$$

and control inputs

$$\tilde{\mathbf{u}}_{long} = \begin{bmatrix} \tilde{\delta}_e \; \tilde{\delta}_{tt} \; \tilde{\delta}_{fb} \; \tilde{\delta}_{vt} \end{bmatrix}^{\mathrm{T}} \tag{2.69}$$

which leads to the longitudinal dynamic equation:

$$\begin{bmatrix} \dot{\tilde{u}} \\ \dot{\tilde{w}} \\ \dot{\tilde{q}} \\ \dot{\tilde{\theta}} \end{bmatrix} = A_{long} \begin{bmatrix} \tilde{u} \\ \tilde{w} \\ \tilde{q} \\ \tilde{\theta} \end{bmatrix} + B_{long} \begin{bmatrix} \tilde{\delta}_e \\ \tilde{\delta}_{tt} \\ \tilde{\delta}_{fb} \\ \tilde{\delta}_{vt} \end{bmatrix} \tag{2.70}$$

with matrices A_{long} and B_{long} defined by Equation 2.62 and Equation 2.63.

Despite not being a longitudinal dynamic state, the altitude can be calculated as an additional integrating state by the equation:

$$\dot{\tilde{h}} = V_{t_e} \tilde{\theta} - \tilde{w} \tag{2.71}$$

3 TRAJECTORY CONTROL

Before talking about the controller development, it is necessary to talk about the mission architecture. Within environmental surveillance applications there are two main branches of study in cooperative robotics: area coverage and target tracking, which are often performed simultaneously (Pimenta *et al.* (2009)). A typical hierarchy of communication and coordination of mission planning that is able to perform both tasks of covering and tracking is shown in Figure 3.1 (Tsourdos *et al.* (2010)). The top layer defines the mission task allocation, the middle layer is the guidance block that defines the trajectories/references to be followed by each UAV, and the lower layer corresponds the local controllers that ensure that the UAVs will execute the commanded trajectories/velocities.

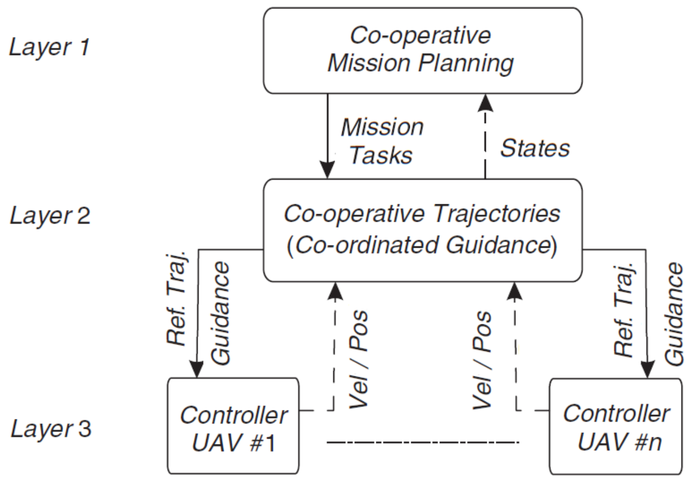

Figure 3.1 Mission Architecture (Adapted from Tsourdos *et al.* (2010)).

s

The mission tasks considered in this Thesis are two (Figure 3.2):

- **Waypoint/Hovering** - The airship receives a target coordinate with an entry angle and the controller takes the airship there, flying at a given altitude and speed. Upon arrival, the airship may proceed to the next point, or it may stay in place (hovering), within a 10 m radius from the targeted point, enabling the airship to face the wind, minimizing air drag. The waypoints (black) and hovering circles (red) are illustrated in Figure 3.2.

- **Target tracking** - Another kind of mission is the tracking of a moving target on the ground, when the airship should follow the interest object keeping a given distance from it.

The coordinated guidance approach (2nd layer) used here is the *leader/follower* technique, very common on UAVs coordinated flight. In this mode, the follower airship should maintain a desired distance and orientation angle from the leader, which allows for a flying formation to be achieved, be it in line flight, column or diagonal ("V" formation). The implementation is a SFKC approach, commonly used in mobile robotics for terrestrial vehicles (Siegwart *et al.* (2011)). Finally, the low level controllers for each UAV is a Sliding Mode Control (SMC), as implemented by Vieira *et al.* (2017).

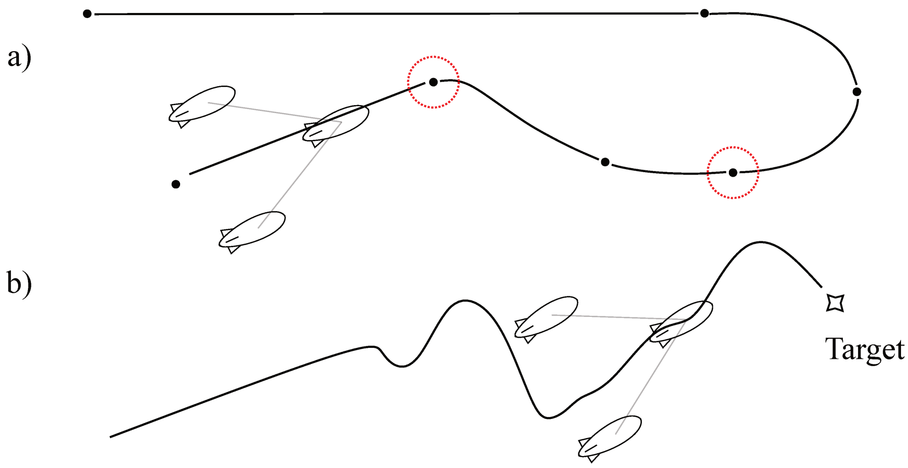

Figure 3.2 Mission Tasks: waypoint path following with or without hovering flight (a) and tracking of moving target (b).

3.1 Second Layer - Kinematic Controller

For the middle layer (guidance), the *leader/follower* approach, although extensively investigated for different kinds of aircrafts, to the best of the author's knowledge, there is only one work in the literature focused on coordinated flight of airships, using the mentioned approach, done by Bicho *et al.* (2006). However, this work is only applied to the waypoint path following case and, besides, the authors do not show the resulting control actuators signals for better analysis and comparison. The idea of the *leader/follower* technique is to impose speed and orientation references for two airships at a time, which may fly in 3 different modes that are: "V", column or line or formation (Figure 3.3). The distance and orientation between the two airships are controlled by keeping the heading and relative speed between both, which is guaranteed by the low level controllers. This structure is then combined to generate more complex formations with an arbitrary number of airships, such as the known "V" formation. Nevertheless, in this work, only three airships are considered, flying together in "V", though the idea of Bicho *et al.* (2006) is extended to cover more complex flight mission cases, such as hovering and moving target tracking.

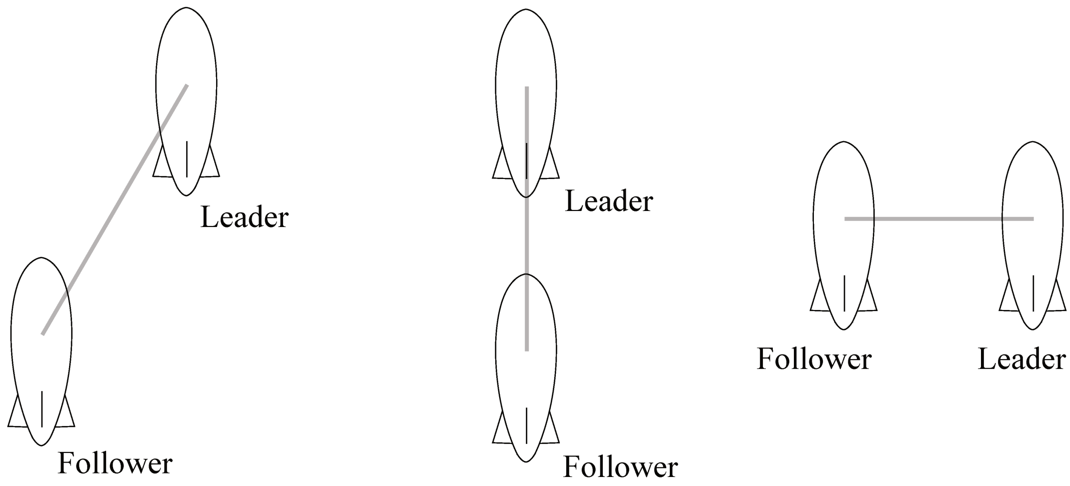

Figure 3.3 Basic airship configurations in a *leader/follower* formation.

Follower control

Recall from chapter 2 that ψ_i is the Euler angle orientation (yaw angle), in the D axis (NED frame) for the *follower* airship and ζ_i the angle between the *leader* and *follower* positions in the same axis. It is desired that the *follower* airship maintains a certain distance, $\rho_{i,d}$, from the *leader*, as well as a certain relative angle, $\zeta_{i,d}$. The solution for this kind of problem of position/orientation control is delegated to the low level controller (3rd layer of Figure 3.1) that is based on a simple kinematic model (Equation 3.1 and Figure 3.4). This SFKC approach is commonly used in mobile robotics for terrestrial vehicles (Siegwart *et al.* (2011)).

$$\begin{bmatrix} \dot{\rho} \\ \dot{\zeta} \\ \dot{\epsilon} \end{bmatrix} = \begin{bmatrix} -\cos\zeta & 0 \\ \frac{\sin\zeta}{\rho} & -1 \\ -\frac{\sin\zeta}{\rho} & 0 \end{bmatrix} \begin{bmatrix} u_{ref} \\ r_{ref} \end{bmatrix} \tag{3.1}$$

Be aware that Equation 3.1 assumed the goal was at the origin of the inertial frame, which does not incur any loss of generality. The complete relations utilized in the simulator were as follows:

$$\rho_i = \sqrt{{\Delta P_E}^2 + {\Delta P_N}^2} - \rho_{i,d} \tag{3.2}$$

$$\zeta_i = -\psi_i + \text{atan}\,\frac{\Delta P_E}{\Delta P_N} - \zeta_{i,d} \tag{3.3}$$

$$\epsilon_i = -\psi_i - \zeta_i + \psi_j \tag{3.4}$$

which takes into consideration that the goal frame is a mobile one. To derive the state feedback gain, first we linearize (Equation 3.1) assuming small-angle errors such that $\cos(\zeta) \simeq 1$ and

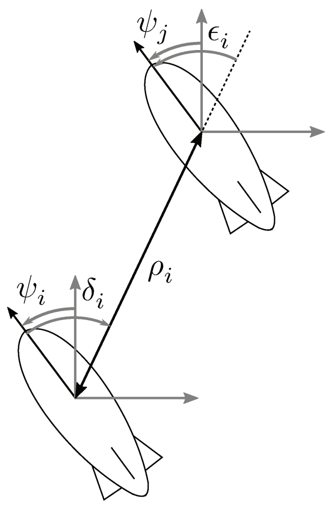

Figure 3.4 Polar coordinate system with the origin set at the NED frame of the leader airship, used in the second layer control (SFKC). This illustration considers $\rho_{i,d} = 0$ and $\zeta_{i,d}$(Adapted from Bicho *et al.* (2006)).

$\sin(\zeta) \simeq \zeta$. The feedback control law defined by Siegwart *et al.* (2011) is:

$$u_{ref} = k_\rho \rho \tag{3.5}$$

$$r_{ref} = k_\zeta \zeta + k_\epsilon \epsilon \tag{3.6}$$

which had the subscripts dropped, in order to ease the notation.

These velocities compose the airspeed reference command sent to the adapted airship kinematic model, that is:

$$\mathbf{u}_{a_{ref}} = [u_{ref}\, 0\, 0\, 0\, 0\, r_{ref}]^{\mathrm{T}}; \tag{3.7}$$

As the use of airspeed control signals infers no loss of generality, the subscript a will not be employed to ease the notation.

The substitution of these control laws in the linearized model of Equation 3.1 leads to the following closed-loop state space model:

$$\begin{bmatrix} \dot{\rho} \\ \dot{\zeta} \\ \dot{\epsilon} \end{bmatrix} = \begin{bmatrix} -k_\rho & 0 & 0 \\ 0 & -(k_\zeta - k_\rho) & -k_\epsilon \\ 0 & -k_\rho & 0 \end{bmatrix} \begin{bmatrix} \rho \\ \zeta \\ \epsilon \end{bmatrix} \tag{3.8}$$

whose dynamic matrix should have stable eigenvalues by the proper choosing of the gains $k_\zeta,\ k_\rho,\ k_\epsilon$. In other words, $k_\rho > 0$, $k_\epsilon < 0$ and $k_\zeta > k_\rho$. Furthermore, Siegwart *et al.* (2011) cites a robust position control, that was implemented in this work, which should prevent the robot from changing direction during its approach to the goal, which is

$$k_\rho > 0; \quad k_\epsilon < 0; \quad k_\zeta > k_\rho; \quad k_\zeta + \frac{5}{3}k_\epsilon - \frac{2}{\pi}k_\rho > 0 \tag{3.9}$$

One addition that was made to the SFKC was a feedforward to aid the velocity tracking of the follower airship. The velocity reference is the true airspeed of the leader airship $V_t = \|\mathbf{v}_a\|_2 = \sqrt{u_a^2 + v_a^2 + w_a^2}$. Being $y_j(k) = [P_{N_j}(k),\ P_{E_j}(k)]^{\mathrm{T}}$ the position of the leader airship at any instant k, then the equilibrium point sought by the follower airship is given by

$$y_{ref}(k) = [P_{N_j}(k) - \rho_{i,d}\cos(\psi_j(k) + \zeta_{i,d}),\ P_{E_j}(k) - \rho_{i,d}\sin(\psi_j(k) + \zeta_{i,d})]^{\mathrm{T}} \tag{3.10}$$

and

$$V_{t_{ref}} = \frac{y_{ref}(k) - y_{ref}(k-1)}{T_s} \tag{3.11}$$

where T_s is the sampling time. This also added a feedforward gain k_{ff} to the controller. With the defined linear conditions, $u_{ref} = V_{t_{ref}}$. This makes the closed-loop state space model

$$\begin{bmatrix} \dot{\rho} \\ \dot{\zeta} \\ \dot{\epsilon} \end{bmatrix} = \begin{bmatrix} -k_\rho & 0 & 0 \\ 0 & -(k_\zeta - k_\rho) & -k_\epsilon \\ 0 & -k_\rho & 0 \end{bmatrix} \begin{bmatrix} \rho \\ \zeta \\ \epsilon \end{bmatrix} + \begin{bmatrix} k_{ff} & 0 \\ 0 & 0 \\ 0 & 0 \end{bmatrix} \begin{bmatrix} u_{ref} \\ r_{ref} \end{bmatrix} \tag{3.12}$$

One of the most interesting properties of this SFKC is that with a single set of tuning control parameters k_ζ, k_ρ, k_ϵ and k_{ff} it is possible to implement, with just some small changes, the different operational modes of waypoint flight, hovering flight and ground tracking flight used to execute the two main missions of waypoint path following and target tracking. Additionally a limit to the angular error was added, where the airship reduces the linear speed $\mathbf{x}_a$ and increases the angular speed $\boldsymbol{\omega}_a$, both to a fixed value. For the “follower” airship in the “leader/follower” guidance approach, the “goal” point in Figure 3.4 will always be the position of its corresponding “leader” airship. And for the main leader airship in the “V” coordinated flight, the goal may be the next waypoint (in the waypoint flight), the hovering waypoint (in the hovering flight) and the target current position in North$\times$East coordinates (in the target tracking). In this last case, the idea is to generate a kind of “walk-stop-walk” behavior to follow the target using both the constant airspeed and the hovering control modes. The airship will follow the target at a constant airspeed and whenever its projected distance to the object reaches the limit of 5 m, it switches to the hovering control.

Leader control

The control of the leader airship was divided in two modes: cruise and approximation mode. The first is used during path following, where the linear velocity $\dot{\rho}$ is defined by feedforward control and the angular states $\dot{\zeta}$ and ϵ are defined by feedback control. Simply put, $\dot{\rho} = k_{ff}u_{ref}$, with $k_{ff} = 1$.

The second control mode is the approximation. It is engaged during hover flight or target tracking. It behaves as the follower control, however the final airship heading ψ will be facing the wind, as this will minimize the air drag. This behavior is illustrated on Figure 3.5. During target tracking, this is the only mode in which the leader operates, but during the waypoint/hover it only engages when $\rho \leq 5\,\text{m}$.

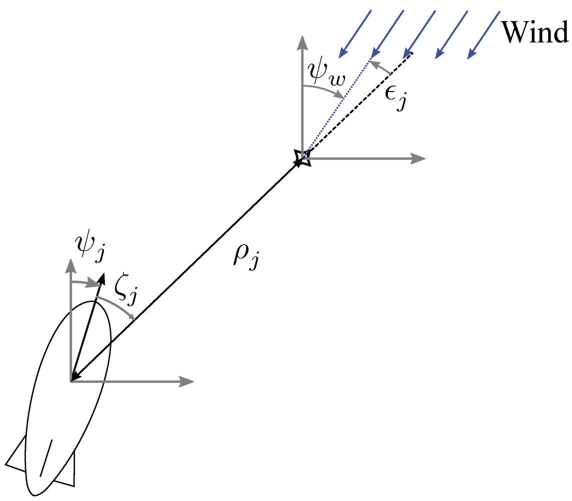

Figure 3.5 Airship approximation mode, during hover flight or target tracking.

Note that the closed loop is only valid in the kinematic model, as the dynamical has a radically different equation. For the former, only the control signals $u_{ref} = k_\rho \rho + k_{ff} V_{t_{ref}}$ and $r_{ref} = k_\zeta \zeta + k_\epsilon \epsilon$ remain valid.

3.2 Third Layer - Sliding Modes Controller

For the third layer of this control architecture, Moutinho (2007) explores linear and nonlinear options. In her work, it is stated that because of the system being linearized around a desired condition, it would not be possible to have a controller that meets the required specifications for ground-hover and target tracking, for example. Since target tracking, path following and ground-hovering are objectives of this work, a nonlinear controller had to be implemented. The

SMC implemented by Vieira *et al.* (2017), manages to control the coupled airship system (lateral and longitudinal motions) while achieving great robustness, given that the system was always stabilized even with the saturation of the actuators and an airspeed variation range of [3–13] $\mathrm{m/s}$ and was chosen as the third layer controller.

The SMC is a particular mode in Variable Structure Systems (VSS). As explained in Shtessel *et al.* (2014), these systems include multiple structures and rules to switch between them, in order to preserve some desired performance that could not be achieved by any of the systems alone. Furthermore, the switch function can drive the system to a special mode, called sliding mode, which presents a particular dynamic, different from those of the subsystems. This dynamic is insensitive to particular model uncertainties, called matched uncertainties, which are uncertainties implicit in the input channels.

The design of the SMC happens in two steps, the definition of the sliding surface and obtaining the control law. As happened in the modeling chapter, the SMC design is rather extensive and only the definition of the linear part of the control law will be presented here. The full development can be found in de Paiva *et al.* (2007), Benjovengo *et al.* (2009), Moriguchi (2017) and Vieira *et al.* (2017). The following development follows the Shtessel *et al.* (2014) book.

Controlled States

Before synthesizing the SMC it is necessary to define the states that will be controlled first. Although Equation 3.8 works well for the kinematic simulator, the introduction of additional states was necessary for the dynamical one. One of the states introduced was the lateral error. For the leader, the definition of the lateral error is trivial, as is simply the smallest distance between the CV of the airship and the straight that connects the last and current waypoints. An angle between the two points can also be defined to make a curved path. During the hover case, it is the central point of the hover area and the wind angle incidence ψ_w that define the straight from which the lateral error will be derived. Target tracking does not have a lateral error defined, as the leader can make no inference from the target trajectory.

For the follower airships, there is no obvious definition for this straight, which opens some possibilities to explore. One of them, and the one utilized, is the straight defined by the current and last point of the leader airship offsetted by $\rho_{i,d}$ and $\zeta_{i,d}$. That is, being $y_j(k) = [P_{N_j}(k),\ P_{E_j}(k)]^{\mathrm{T}}$ the position of the leader airship at any instant k, then the equilibrium point sought by the follower airship is given by

$$y_{ref}(k) = [P_{N_j}(k) - \rho_{i,d}\cos(\psi_j(k) + \zeta_{i,d}),\ P_{E_j}(k) - \rho_{i,d}\sin(\psi_j(k) + \zeta_{i,d})]^{\mathrm{T}} \tag{3.13}$$

and the straight is defined by linear combination of $y_{ref}(k)$ and $y_{ref}(k-1)$. Figure 3.6 illustrates this definition.

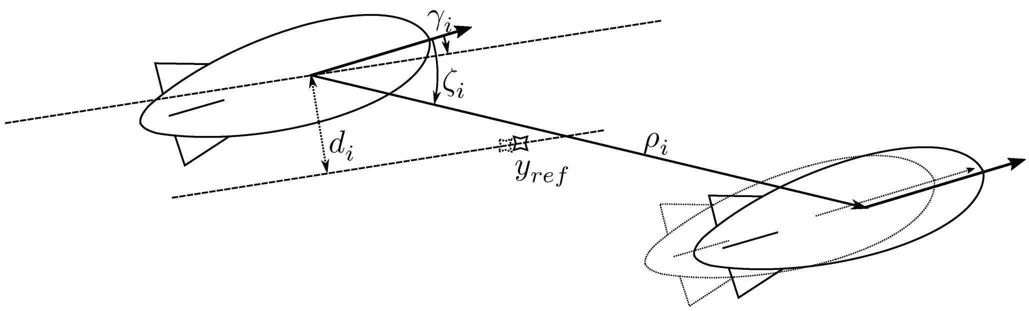

Figure 3.6 Superior view (North×East) of the lateral trajectory error for the follower airship. The reference straight is drawn from the current and last reference point. The point is simply the point where the follower airship is at equilibrium, that is, Equation 3.2 and 3.3 are zero (Adapted from de Paiva *et al.* (2007)).

Figure 3.6 also shows the other new state, which is γ, the angular error between the velocity of the airship u and the described straight. There are already so many angles defined on the horizontal plane that this one may seem unnecessary at first, however, it is used to describe the lateral error d, rather than for control purposes.

Besides the extended states, there are also the states described in Equation 2.66 and Equation 2.70 to be considered. The states that Vieira *et al.* (2017) chose to control and that are utilized here are:

$$\mathbf{x}_{lat_{ctrl}} = [\tilde{r}\ \tilde{\varphi}\ d_i] \tag{3.14}$$

for the controlled lateral states and

$$\mathbf{x}_{long_{ctrl}} = \left[\tilde{u}_a\ \tilde{w}_a\ \tilde{q}\ \tilde{\theta}\ \tilde{h}\right] \tag{3.15}$$

SMC - Control Law Design

In order to design a SMC, the linear model from Equation 2.61 is utilized. The referred equation, repeated here to facilitate the reading, is

$$\dot{\tilde{x}} = A\tilde{x} + B\tilde{u} + B\xi \tag{3.16}$$

with $A \in \mathbb{R}^{n\times n}$, $B \in \mathbb{R}^{n\times m}$, $x = \left[\mathbf{v}^{\mathrm{T}}\ \mathbf{p}^{\mathrm{T}}\right]^{\mathrm{T}}$, $u = \left[\mathbf{u}_{long}^{\mathrm{T}}\ \mathbf{u}_{lat}^{\mathrm{T}}\right]^{\mathrm{T}} = [\delta_e\ \delta_{tt}\ \delta_{fb}\ \delta_{vt}\ \delta_r\ \delta_{cd}]^{\mathrm{T}}$ (which defines $n = m = 6$) and ξ is the differences between the linear and nonlinear models, unaccounted for in the referenced equation.

Let the switching function $\sigma : \mathbb{R} \to \mathbb{R}^m$ be

$$\sigma(\tilde{x}) = S\tilde{x} = [S_1\ S_2]\begin{bmatrix}\tilde{\mathbf{v}}\\ \tilde{\mathbf{p}}\end{bmatrix} \tag{3.17}$$

with $S \in \mathbb{R}^{m\times n}$ being a full rank matrix and $\mathcal{S}$ the hyperplane defined by

$$\mathcal{S} = \{x \in \mathbb{R}^n\ :\ Sx = 0\} \tag{3.18}$$

The main idea is to define the control law, represented by u, and the switching function $\sigma(\tilde{\mathbf{x}})$ so that the sliding motion happens on the $\mathcal{S}$ hyperplane, that is, there is a time t_r in which

$$\sigma(\tilde{x}) = S\tilde{x}(t) = 0, \quad \forall t \geq t_r \tag{3.19}$$

At time $t \geq t_r$ the system lies is on $\mathcal{S}$ at an ideal sliding motion, which is expressed by $S\tilde{x}(t) = 0$ and $\dot{\sigma}(x) = S\dot{\tilde{x}}(t) = 0$. Multiplying Equation 3.16, at $t \geq t_r$, by S yields

$$S\dot{\tilde{x}} = SA\tilde{x} + SB\tilde{u} + SB\xi = 0 \tag{3.20}$$

and the unique solution is the equivalent control

$$u_{eq} = -(SB)^{-1}SA\tilde{x} - \xi \tag{3.21}$$

Substituting u_{eq} in Equation 3.16 gives

$$\dot{\tilde{x}} = (I_n - B(SB)^{-1}S)A\tilde{x} \tag{3.22}$$

With the way that x and u were defined, SB does not have an inverse, as $B = \left[B_1^{\mathrm{T}}\ 0_{6,3}\right]^{\mathrm{T}}$. The solution to this problem is simply to use the pseudo-inverse, as done by Vieira *et al.* (2017).

The control law, for now, only comprises the linear part so far, however a discontinuous part is sought to force $\sigma \to 0$ in finite time. To put in a straightforward manner, the objective is to turn the equation

$$\dot{\sigma} = S\dot{\tilde{x}} = SA\tilde{x} + SB\tilde{u} \tag{3.23}$$

into the differential equation

$$\dot{\sigma}_i = -\eta_i \operatorname{sgn}(\sigma(\tilde{x})) \tag{3.24}$$

this part of the development will not be shown here, as not to needlessly extend this chapter. As stated above, the full development can be found in Shtessel *et al.* (2014).

The control law found for this system, as defined by Vieira *et al.* (2017) is

$$u = -(SB)^{+}SA\tilde{x} - (SB)^{+}\dot{\sigma}_i \tag{3.25}$$

with $(SB)^{+}$ being the pseudo-inverse of SB and $\dot{\sigma}_i$ the same one defined in Equation 3.24. The global stability of σ has been proved in de Paiva *et al.* (2007).

SMC - Chattering

A problem that derives from this method is that the switching function must approach an infinite frequency to achieve total uncertainty rejection. As the control signal is a discontinuous one, the high-frequency switching causes chattering (Figure 3.7), which leads to slow processing in simulations and potentially causes damages to real world mechanical or electrical implementations.

To avoid chattering, Vieira *et al.* (2017) redefined $\dot{\sigma}$ as

$$\dot{\sigma} = \eta_i \tanh\left(\frac{\sigma(\tilde{x})}{\Psi_i}\right) \tag{3.26}$$

with Ψ being a smoothing factor for the chattering. This, however, changes the asymptotic stability into a bounded stability.

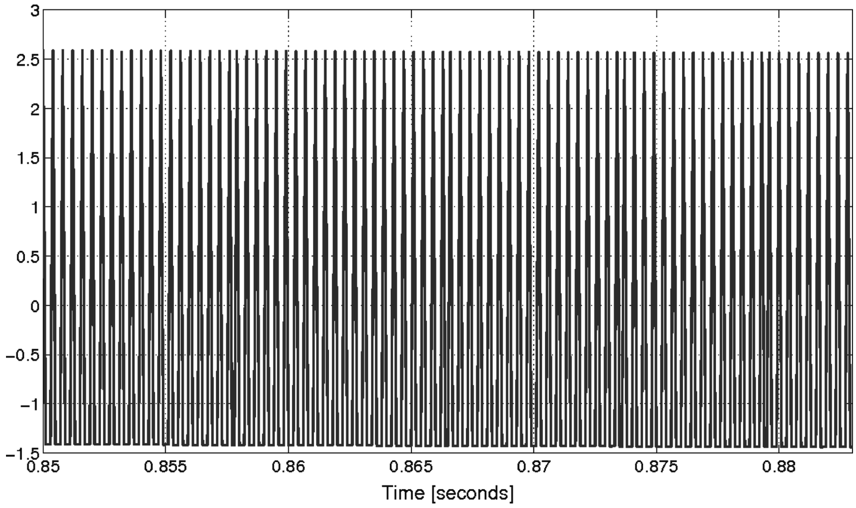

Figure 3.7 Sliding mode control. Zoom of the chattering phenomenon (Shtessel *et al.* (2014)).

SMC - Gain scheduling

The dynamical conditions of the airship are extremely nonlinear. There are saturations and dynamics on the actuators; a naturally elevated inertia, due to the airship form factor; high lateral wind drag; added mass due to air displaced; underactuation on the side of the airship and many more complications. That is to say that, despite being able to reject any uncertainty or perturbations, the gains calculated for a certain trim condition can have poor performance on different conditions, sometimes even saturating the controller. For that reason, it was decided to utilize a minimization function, described in the following algorithm:

Algorithm: trimMinimization($\mathbf{u}_{a_u}$, V_{t_e}, SMCgains)

1: $\tilde{V}_t \leftarrow \mathbf{u}_{a_u} - V_{t_e}$ % Vector V_{t_e} will be subtracted of scalar u_{a_u}
2: $[\sim, I] \leftarrow \min(|\tilde{V}_t|)$ % The absolute value of each element of V_t is calculated and the index of the smallest is saved
3: $k_{SMC} \leftarrow \text{SMCgains}(I)$ % The gains of the SMC for that trim condition are selected and saved
4: **return** k_{SMC}

In other words, a scheduler was implemented for the first time for an airship - even though it was out of the scope of this work - to select the most appropriate gains at each instant of simulation. Between 0 and 15 m/s, there was 74 trim conditions utilized by Vieira *et al.* (2017) and all of which are possible to use in the implemented controller. These trim points constitute the V_{t_e} vector, while SMCgains is another vector that contains 74 sets of gains for the SMC controller, related to each trim point.

4 KINEMATIC SIMULATOR

There is, currently, two versions of airship simulators. One which implements the kinematic model and the other, that implements the dynamical model. In this chapter, only the former will be explained, as it was used as a middle step to lay the foundations of much more complex control techniques, implemented in the latter. The differences between the kinematic and dynamical simulators are the equations utilized to calculate all the airship states and the number of states themselves.

For simulation purposes, the airship kinematic model needs to be adapted in order to reflect a more realistic behavior including emulation of saturation/dynamics of actuators and the underactuation in lateral movement. The solution was to add a first-order dynamic to the airship position, making the current airspeed $\mathbf{x}_a(k)$ a convex combination between the reference airspeed $\mathbf{x}_{a_u}(k)$ and previous airspeed $\mathbf{x}_a(k-1)$. The block diagram of Figure 4.1 and the algorithm below summarizes this adapted kinematics.

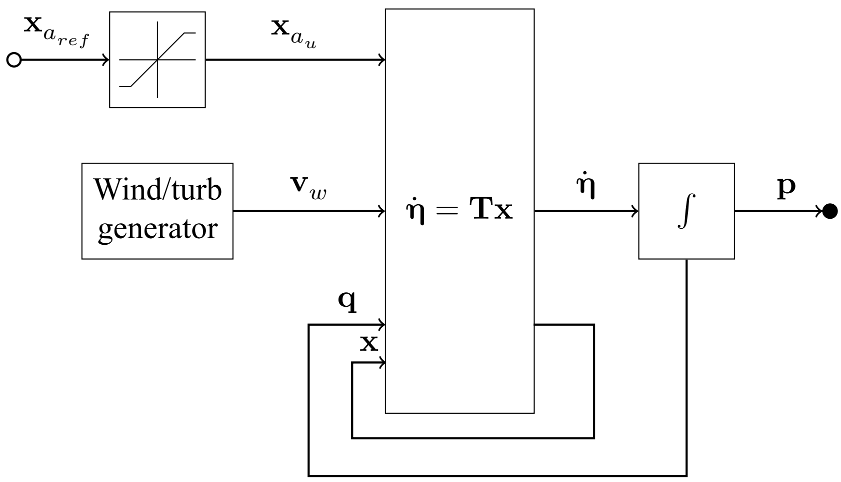

Figure 4.1 Adapted airship open-loop kinematic model for simulation.

Algorithm: kinSimulation($\mathbf{x}_{a_u}, \mathbf{v}_w, \mathbf{q}, \mathbf{x}$)

$[\mathbf{S}, \mathbf{T}] \leftarrow$ transformationMatrices($\mathbf{q}$, $\boldsymbol{\omega}$)
$\mathbf{x}_w \leftarrow [\mathbf{S} \times \mathbf{v}_w \ 0 \ 0 \ 0]$
$\mathbf{x}_a \leftarrow \mathbf{x} - \mathbf{x}_w$
$\mathbf{x}_a \leftarrow \alpha \, \mathbf{x}_{a_u} + (1-\alpha) \, \mathbf{x}_a$
$\mathbf{x} \leftarrow \mathbf{x}_a + \mathbf{x}_w$
$\dot{\boldsymbol{\eta}} \leftarrow \mathbf{T} \, \mathbf{x}$
$\boldsymbol{\eta} \leftarrow \int \dot{\boldsymbol{\eta}}$
return $(\mathbf{x}, \mathbf{q}, \boldsymbol{\eta})$

Recall that the input command to the airship $\mathbf{x}_{a_u} = \left[u_{a_u} \ v_{a_u} \ w_{a_u} \ p_{a_u} \ q_{a_u} \ r_{a_u}\right]^{\mathrm{T}}$ is the saturated vector of linear $(u_{a_{ref}}, \ v_{a_{ref}}, \ w_{a_{ref}})$ and angular $(p_{a_{ref}}, \ q_{a_{ref}}, r_{a_{ref}})$ desired airspeed velocities, coming from the airship guidance controller, detailed in the next section. The algorithm can be summarized as follows: Assuming that the wind speed in global coordinates is known ($\mathbf{v}_w = [t_w \; v_w \; w_w]^{\mathrm{T}}$) from the perturbation input, then the current airspeed vector in local frame ($\mathbf{x}_a = [\mathbf{v}_a^{\mathrm{T}} \; \boldsymbol{\omega}_a^{\mathrm{T}}]^{\mathrm{T}}$) is calculated. A weighting parameter (α) is utilized to recalculate $\mathbf{x}_a$, combining the commanded airspeed ($\mathbf{x}_{a_u}$) and the previously calculated airspeed ($\mathbf{x}_a$). This introduces a first order dynamics on the commanded airspeed, emulating the dynamics from the airship actuators. Moreover, as the weighting factor α is small, it imposes a priority to the current airspeed vector. This allows, for example, for abrupt changes in the airspeed due to a sudden wind incidence. With the airspeed vector defined in this way, it is possible to calculate a realistic groundspeed vector, as well as the airship position and quaternions in the global frame.

As for the simulator itself, it is organized in a fairly simple manner. For the sake of easing the text, each airship will be simply called DRONI. Each DRONI node is a complete airship simulator. In Figure 4.2, DRONI 1 is the leader, while both DRONI 2 and DRONI 3 follow the leader, as opposed to DRONI 3 following DRONI 2. The Moving target node was commented out to change to waypoint mode.

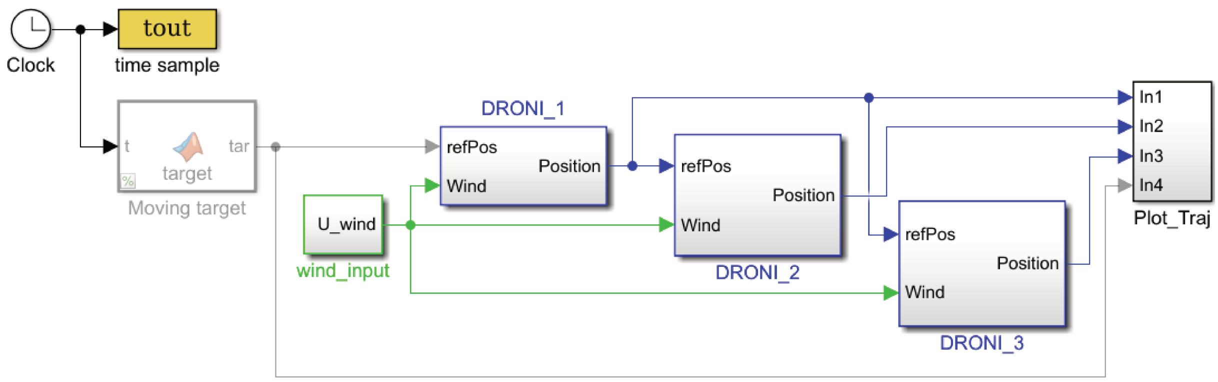

Figure 4.2 Simulink model for the kinematic simulators, implementing both moving target and waypoint/hovering missions, Dryden wind/turbulence model.

The Figure 4.4 illustrates in a simplified way what is represented in Figure 4.3, that is, the design of each DRONI node. The second layer block calculates the trajectory that the airship must follow and feed this information to the third layer controller, which is inside a tradition control loop, with negative feedback. The wind enters as a disturbance and this inside loop can only react to it. Specifically for the hovering case, the second layer controller keeps the airship orientation directly against the wind, to minimize drag. What is not illustrated in this diagram is the second layer loop, as it is not a simple control loop, but rather an algorithm. The first layer role is played by the script that runs the simulator and is also not represented in this figure.

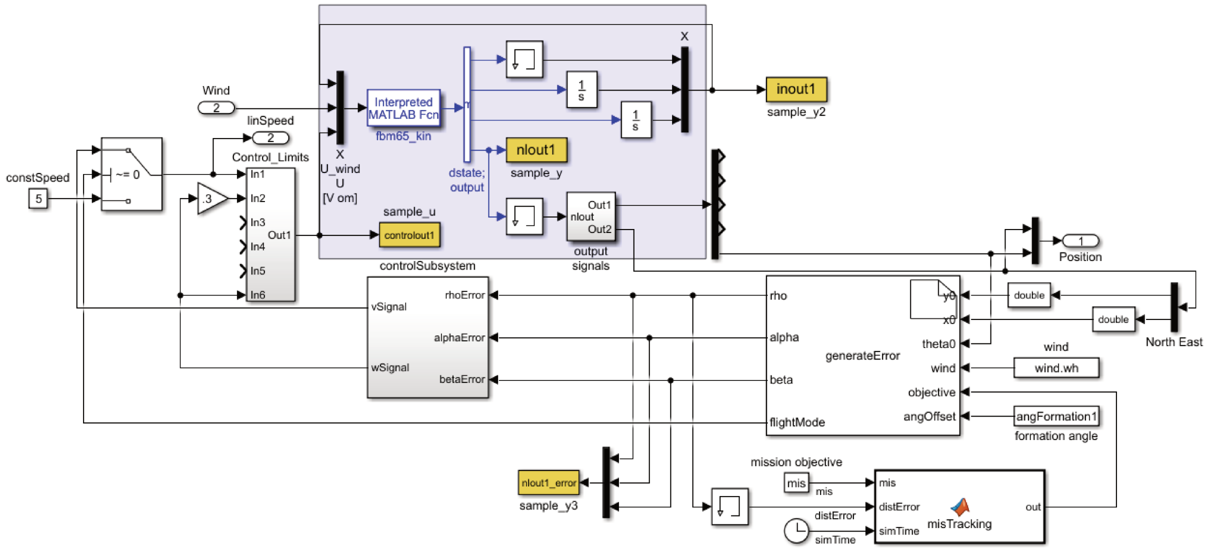

Figure 4.3 Simulink model for the each individual Droni. The shaded area is the entire model implementation, with the exterior being the control loop and data collecting.

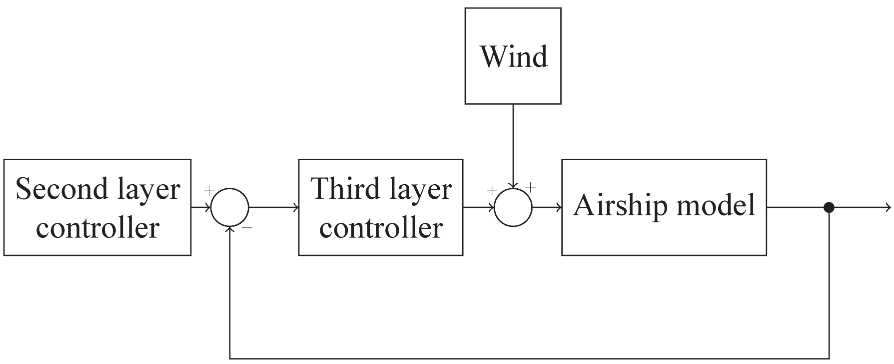

Figure 4.4 Simplified inner control loop for the airship simulator

5 SIMULATION RESULTS

5.1 Kinematic Simulations

In order to tune the SFKC a standard mission was set, where an extensive search was made on the k_ρ and k_ζ gains, while k_ϵ was set according to the Equation 3.9. More specifically, $k_\epsilon = (\frac{2}{\pi}k_\rho - k_\zeta + 0.1)\frac{3}{5}$, being 0.1 simply a small term to obey the inequality. The objective here was to minimize the average ρ_e error.

The mission consisted in a simple waypoint circuit, with initially no wind/turbulence. At 20 s of simulation, a sudden wind is cast at Droni 2 only, at $3\,\mathrm{m/s}$ from 30° North, stopping at 50 s. The simulation ends with 70 s. The controller saturation limits were $u = [0, 9]\,\mathrm{m/s}$ and $r = [-20, 20]\,°/\mathrm{s}$. If the angular error passes 90°, r is set to $20\,°/\mathrm{s}$ and u to $3\,\mathrm{m/s}$. The value of α used in the adapted kinematic algorithm was $\alpha = 0.05$. The wind condition was turbulence with a standard deviation of $1\,\mathrm{m/s}$ plus a constant wind of $3\,\mathrm{m/s}$ coming from 30° North. The airship reference altitudes for the three airships (Droni 1, Droni 2, Droni 3) were defined as $h = [50, 60, 70]\,\mathrm{m}$, respectively. The reference distance between follower and leader is set to $\rho_{i,d} = 5\,\mathrm{m}$ and the reference longitudinal airspeed of the airship u is set to $5\,\mathrm{m/s}$. Figure 5.1 shows the best case of all the tests.

The utilized formula to calculate the error, for a mission with duration T, was:

$$\bar{\rho} = \frac{1}{T}\int_0^T \sqrt{\rho_2^2 + \rho_3^2}\,\mathrm{d}t \tag{5.1}$$

being $\bar{\rho}$ is the average error and $\rho_i = \sqrt{\Delta P_E{}^2 + \Delta P_N{}^2} - \rho_{i,d}$ is the same as defined in Equation 3.2. The final result was an average error of 4.55 m and a standard deviation of 1.67 m. Figure 5.2 is a plot of this errors with respect to time.

The following simulations are the worst cases that the SFKC was still able to converge towards the desired equilibrium. Both of the situations had turbulent wind with a standard deviation of $1\,\mathrm{m/s}$ plus a constant wind of $3\,\mathrm{m/s}$ coming from 30° North throughout all the simulation applied to all airships.

Figure 5.3 shows the simulation of the waypoint navigation including eventual hovering points (red circles). It is possible to see that without path planning, the airships keep making round flights around the target until its heading is the same as desired. Also, without any information about the mission or the leader, that they cannot obtain from their sensors, the follower airships had an average of position error of $13.74\,\mathrm{m}$ and a standard deviation of 2.87 m. The errors are

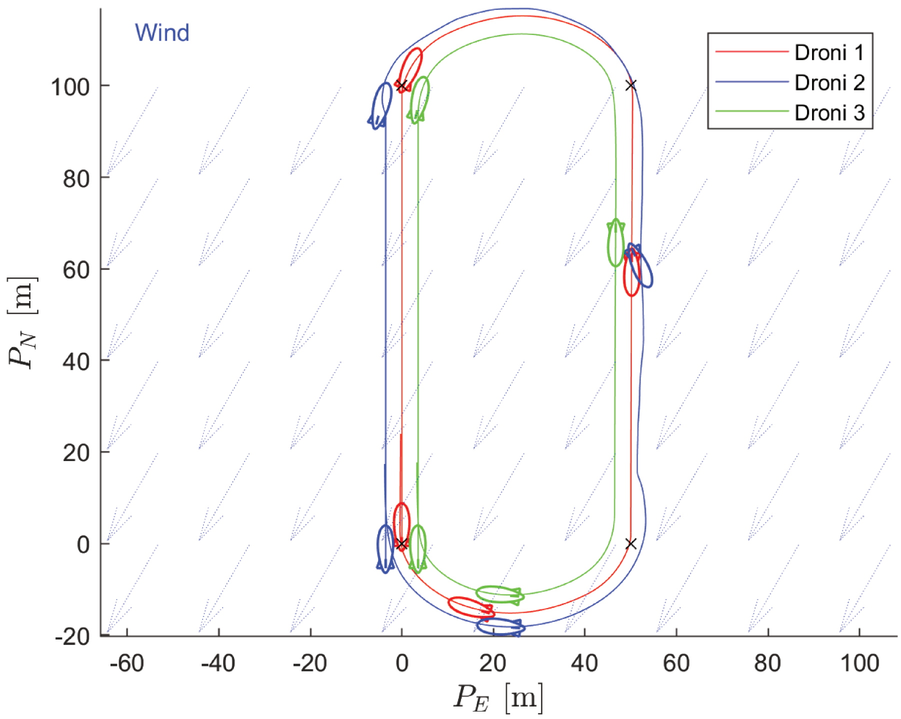

Figure 5.1 Airships in the standard waypoint navigation, used to tune the control gains. The airships are drawn every 20 seconds. Wind is cast at Droni 2 at time 20 s. There was an average error of the distance between the follower airships and their reference positions of 4.55 m and a standard deviation of 1.67 m.

shown in Figure 5.4

Figure 5.5 shows the leader Droni 1's controller inputs and outputs signals. It is possible to see that the commanded airspeeds in u and r are well followed. Note also that the aerodynamic sideslip angle β achieves large values in some moments, due to the maneuvering situations where it gets sideways with the wind incidence.

The last simulation, shown on Figure 5.6, illustrates the case of moving target tracking and Figure 5.8 shows the corresponding leader's signals. The leader is told to follow a ground target and it does that by engaging hovering mode. This way, whenever the target is within a 10 m radius, the airship will keep still and try to face the wind. With more than 10 m, the leader will accelerate trying to close the distance. In this mission, the target is a point with a random movement, modeled as follows:

$$\begin{bmatrix} \dot{P}_N \\ \dot{P}_E \\ \dot{\Psi} \end{bmatrix} = \begin{bmatrix} \cos(\Psi) & 0 \\ \sin(\Psi) & 0 \\ 0 & 1 \end{bmatrix} \begin{bmatrix} v \\ \omega \end{bmatrix} \tag{5.2}$$

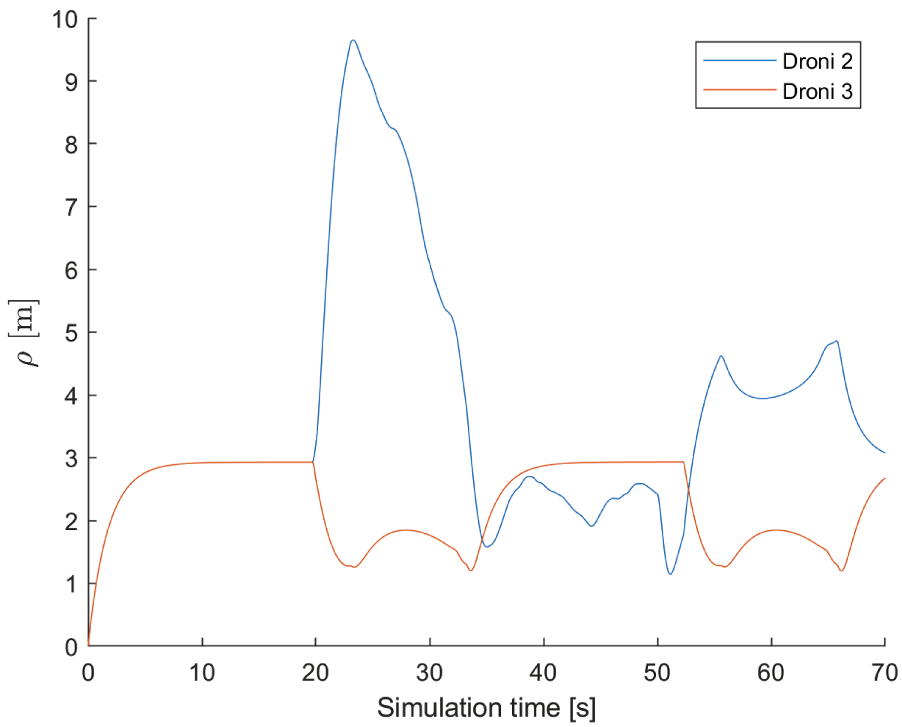

Figure 5.2 Error plot of the follower airships in standard waypoint navigation (Figure 5.1), used to tune the control gains. Wind is cast at Droni 2 at time 20 s. The average of the combined error is 4.55 m and the standard deviation 1.67 m.

where $v = 4\,\mathrm{m/s}$ and ω is a random number, with a continuous uniform distribution, in the interval $[-\pi/10\ ;\ \pi/10]$ rad/s. $P_D = 0\,\mathrm{m}$ always, as the target is grounded. The model is referenced in the NED frame.

Unlike the previous mission, the leader also does not have information about the target, that it cannot obtain from its sensors. The leader had an average error of 13.67 m and a standard deviation of 10.65 m, while the follower airships had an average of position error of 31.02 m and a standard deviation of 24.45 m. The error distribution from the followers is shown on Figure 5.7 and from the leader is shown on Figure 5.9.

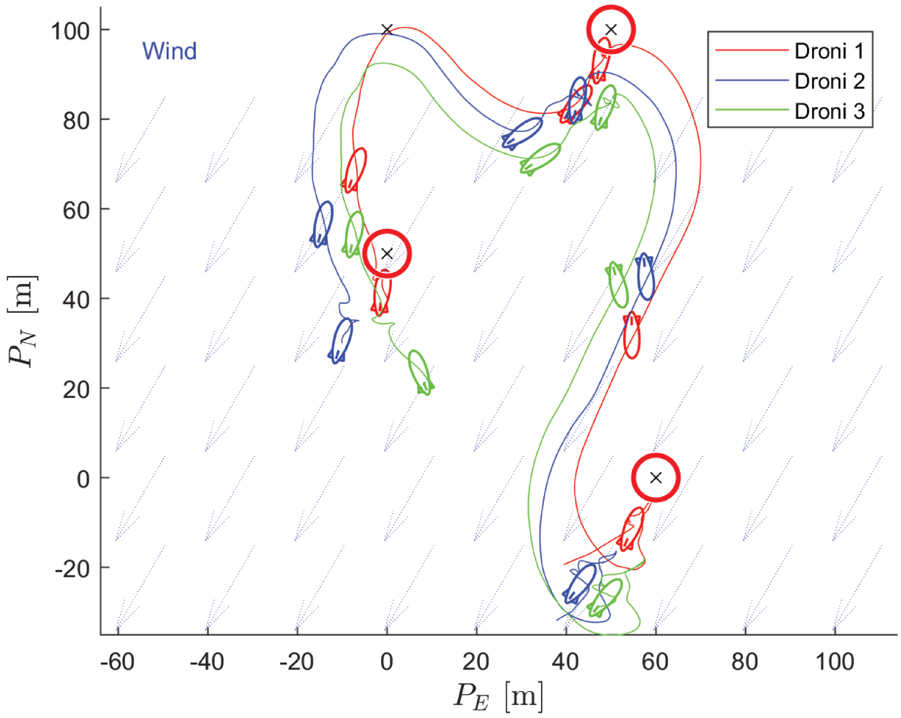

Figure 5.3 Airships in Waypoint/Hovering mode. The red circles are the hovering areas. The airships are drawn at 0, 20, 40, 60, 80 and 150 seconds, to avoid cluttering the final hover spot. There was an average error of the distance between the follower airships and their reference positions of 13.74 m and a standard deviation of 2.87 m.

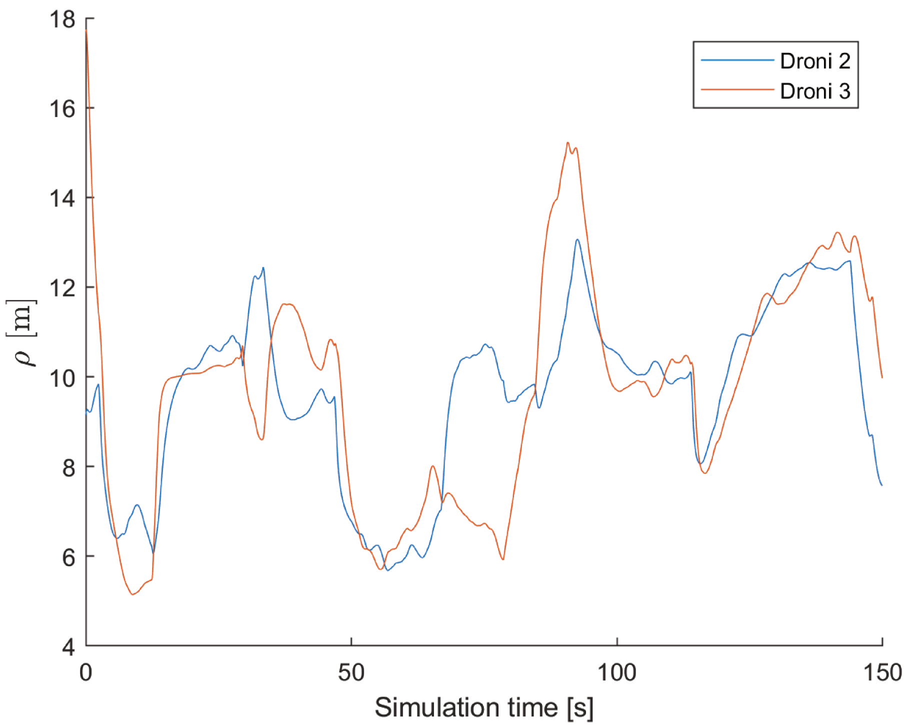

Figure 5.4 Error plot of the follower airships in Waypoint/Hovering mission (Figure 5.3). The average of the combined error is 13.74 m and the standard deviation 2.87 m.

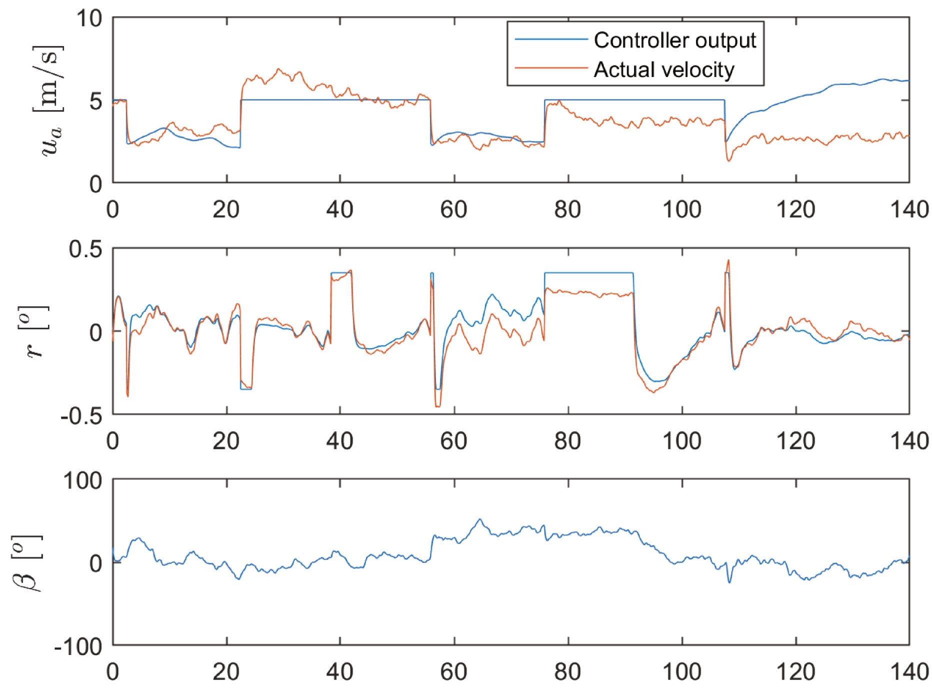

Figure 5.5 Leader's control signals and attack angle (β) during Waypoint/Hover mission (Figure 5.3).

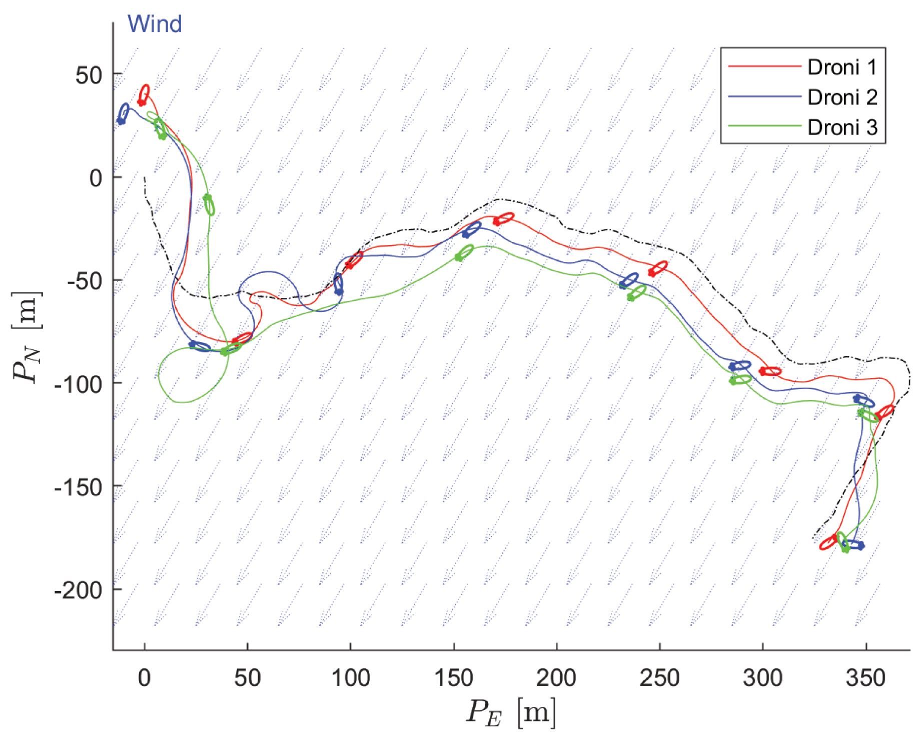

Figure 5.6 Airships in target tracking mission. The airships are drawn every 20 seconds. There was an average error of the distance between the follower airships and their reference positions of 31.02 m and a standard deviation of 24.45 m.

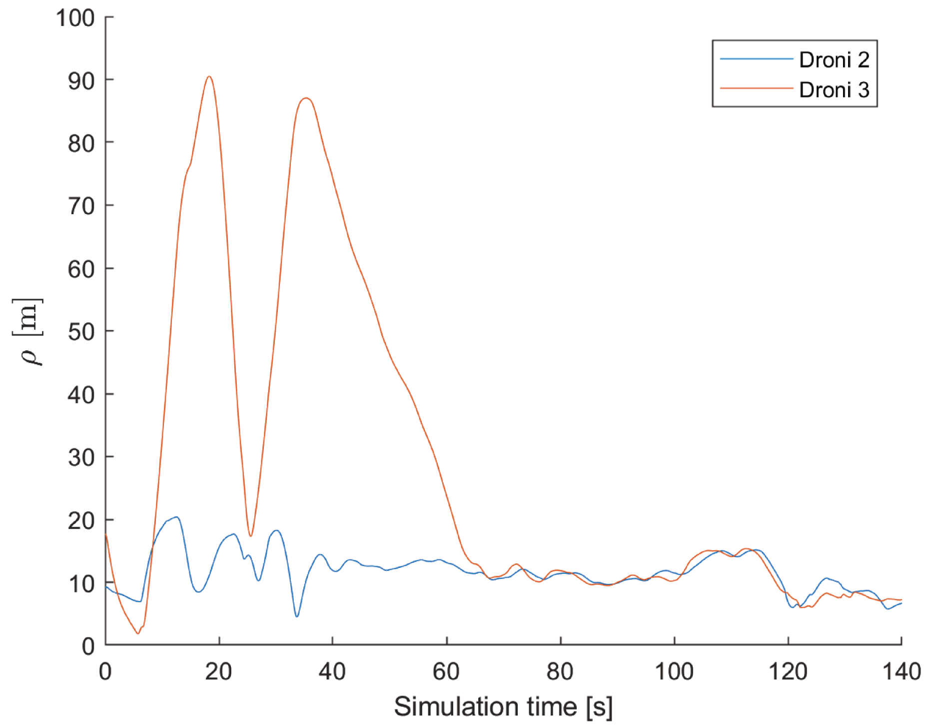

Figure 5.7 Error plot of the follower airships in moving target mission (Figure 5.6). The average of the combined error is 31.02 m and the standard deviation 24.45 m.

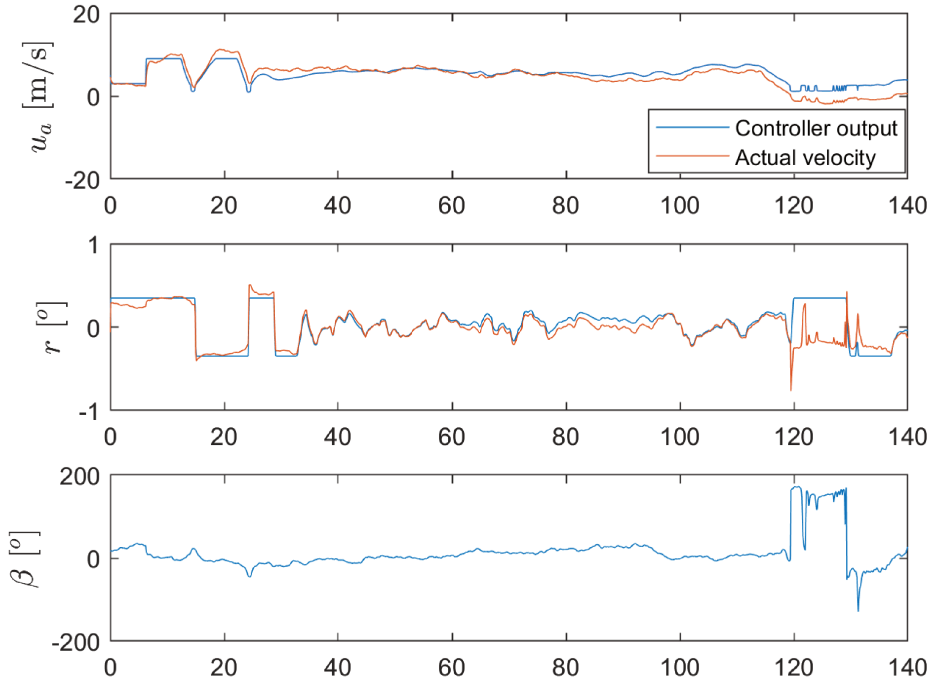

Figure 5.8 Leader's control signals and attack angle (β) during target tracking (Figure 5.6).

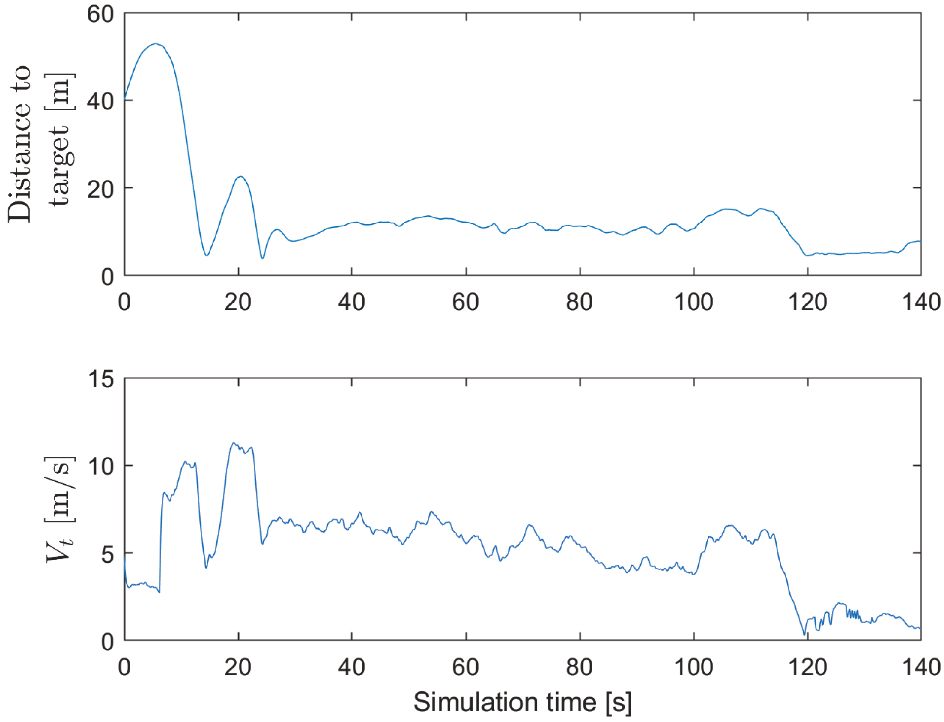

Figure 5.9 Leader's error and total velocity signals during target tracking (Figure 5.6).

5.2 Dynamic Simulations

The first simulations were made with a direct implementation of the kinematic controller, simply retuning the gains to minimize the errors, utilizing the defined mission explained in the beginning of this chapter, with the same duration of 70 s. The linear gain was changed to $k_\rho = 0.4$ while the angular gains changed to $k_\zeta = 3$ and $k_\epsilon = -1.59$. Figure 5.10 shows the last results of this simulation. The waypoints are the same that were used in Figure 5.1. The controller saturation for the linear speed was set as $u = [2, 6]\,\mathrm{m/s}$, while r had no saturation, leaving the limit for the actuators natural saturation. Exactly like the kinematic simulation, there was no wind/turbulence initially, but at time 20 s, a sudden wind of $1\,\mathrm{m/s}$ of standard deviation (turbulence) plus a constant wind of $3\,\mathrm{m/s}$ coming from 30° North is cast at Droni 2 only, ending at 50 s. The airship reference altitudes for the three airships (Droni 1, Droni 2, Droni 3) were defined as $h = [50, 60, 70]\,\mathrm{m}$, respectively. The reference distance between follower and leader is set to $\rho_{i,d} = 5\,\mathrm{m}$ and the reference longitudinal airspeed of the airship u was set to $5\,\mathrm{m/s}$.

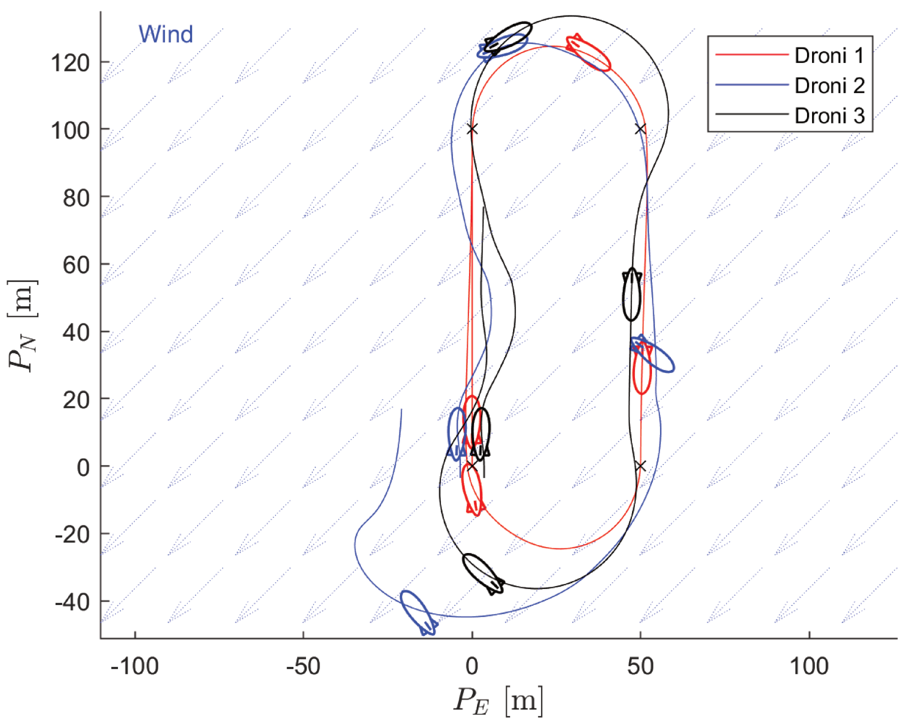

Figure 5.10 Dynamical simulation of the airships in the standard waypoint navigation, used to tune the control gains. The airships are drawn at 0, 20, 40 and 60 seconds.

It was expected that the use of the dynamical model would yield bigger errors than with the kinematic model, however the controller was simply not able to maintain the formation during a flight with no disturbances. For that reason, a better control technique was not only desired, but necessary. This lead to the extended states explained in section 3.2.

The new controller most important addition was the lateral controller, shown in Figure 3.6. It allowed for the inclusion of path planning, which eases the work done by the controller and, in consequence, by the actuators. Even so, its inclusion was not enough. Figure 5.11 shows the first simulation after retuning the controller gains. After the first hover, the follower airships passed the leader and only resumed formation on the last curve. That means that on a 1.03 km path, the airships were on formation for just 200 m, that is, less than 20 % of the mission. Even just considering the errors, the average linear error for the followers was 23.93 m with a standard deviation of 18.72 m. Figure 5.12 shows the error distribution on time.

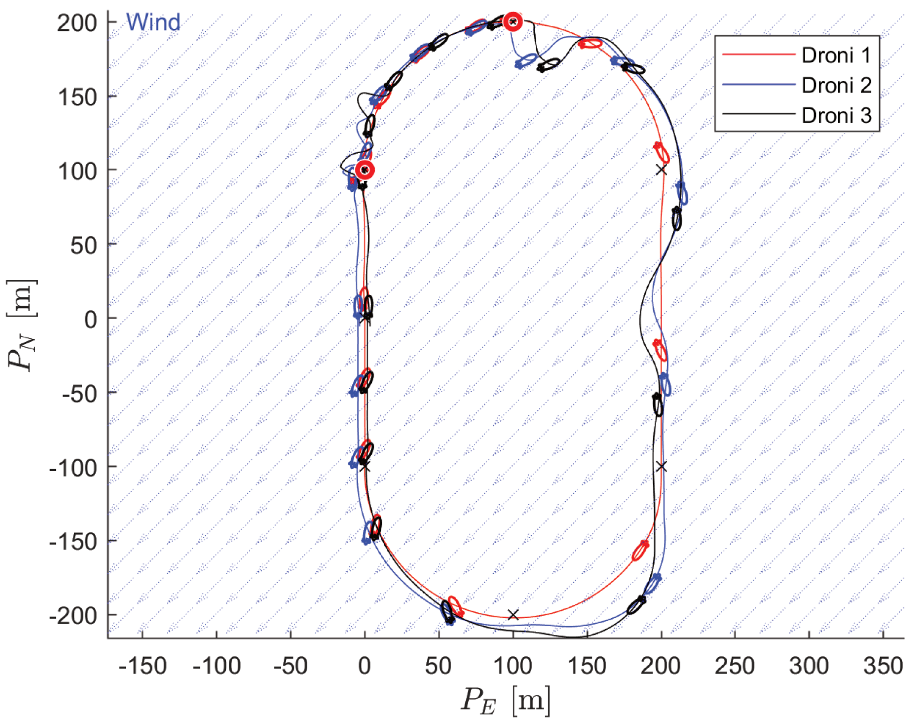

Figure 5.11 Airships in Waypoint/Hovering mode with an on development controller, after the lateral error was introduced. The red circles are the hovering areas. The airships are drawn at every 20 seconds. There was an average error of the distance between the follower airships and their reference positions of 23.93 m and a standard deviation of 18.72 m.

Before achieving smaller errors, the second layer controller incorporated an integral gain for the distance error, a saturation for the controller inputs, a feedforward gain from the velocity of the leader and a gain scheduling for the SMC which, to the author’s knowledge, has not yet been implemented for airships. The aforementioned additions introduced parameters that took over sixty simulations to finely tune. The results of this effort follows.

Figure 5.13 shows the simulation of the waypoint navigation including eventual hovering

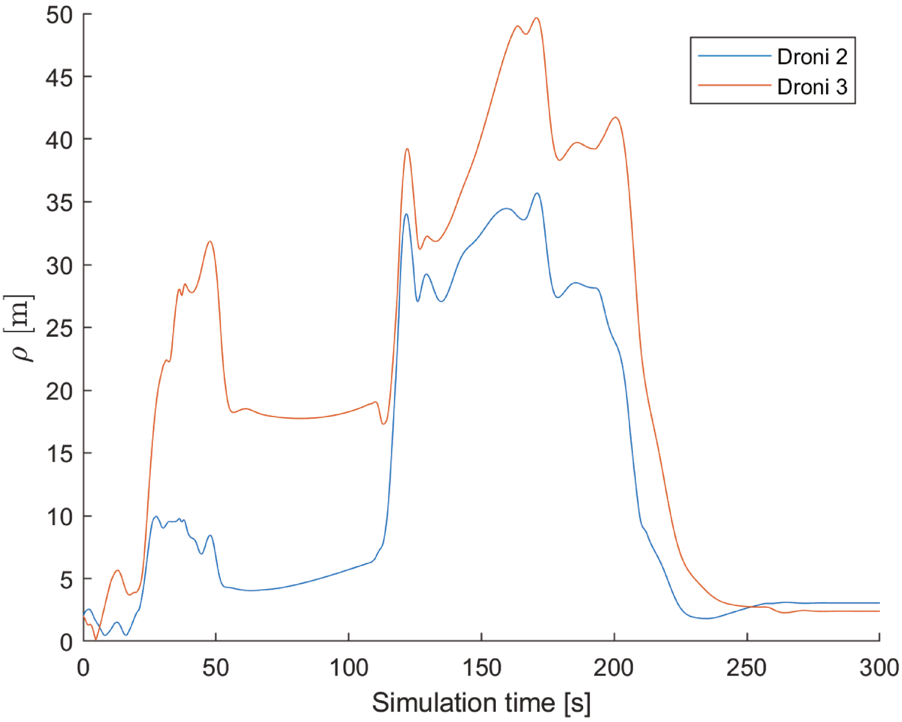

Figure 5.12 Error plot of the follower airships in Waypoint/Hovering mission (Figure 5.11) with an on development controller, after the lateral error was introduced. There was an average error of the distance between the follower airships and their reference positions of 23.93 m and a standard deviation of 18.72 m.

points (red circles). The mission duration was 300 s. It is possible to see the difference that the lateral error made on the path, when comparing to Figure 5.3, where the airship only minimized its error between its heading and the target position. Like the kinematic case, the follower airships only had information, about the leader, that they could sense, without any information about the mission. Despite that, they are able to trace a straight that represented the instantaneous velocity of the leader airship, which allowed them to keep track of their lateral errors. As the leader tends to have lateral errors during flight, the follower airships multiply that errors during the mission, i.e. their flight stability depends directly on the leader stability. The follower airships had an average of position error of 4.61 m and a standard deviation of 4.94 m. The errors are shown in Figure 5.14

Figure 5.15 shows the leader Droni 1's controller inputs and outputs signals. It is possible to see that the commanded airspeed in u_a is well followed. The r speed, however, seems to be not followed at all. The cause of that is the addition of the lateral error, which has a larger influence on state r than the reference input. The lateral error is shown on Figure 5.16 and will substitute the angle r plot, as it does not aid in analysis anymore. Despite that, removing the reference input

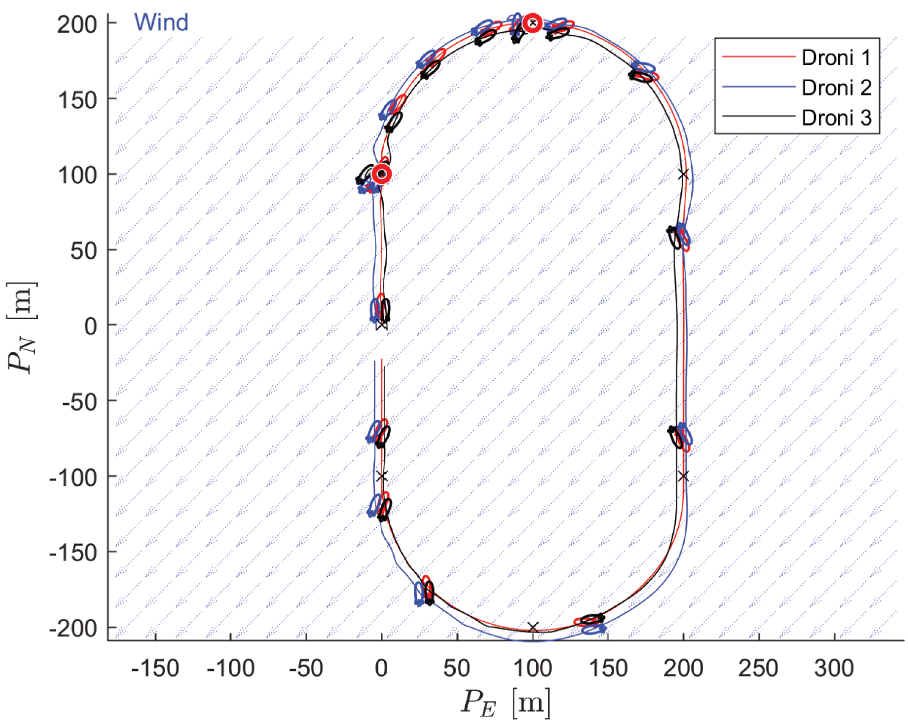

Figure 5.13 Airships in Waypoint/Hovering mode. The red circles are the hovering areas. The airships are drawn at every 20 seconds. There was an average error of the distance between the follower airships and their reference positions of 4.61 m and a standard deviation of 4.94 m.

causes the airships to become unstable. The aerodynamic sideslip angle β also achieves much smaller values than those in Figure 5.5. This comparison may seem unfair, as the first mission seem considerably harder, due to the last hover point, which the airships approach in favor of the wind, however the controller that is now utilized would not make this approach, instead planning a path

The last simulation, shown on Figure 5.17, illustrates the case of moving target tracking and Figure 5.19 shows the corresponding leader's signals. The performance obtained by the leader here is comparable to the kinematic case. The followers also had a good performance, even though their errors were larger than leader had. In this mission, the leader is told to follow a ground target and it does that by engaging hovering mode. This way, whenever the target is within a 10 m radius, the airship will keep still and try to face the wind. With more than 10 m, the leader will accelerate, trying to close the distance.

Unlike the previous mission, the leader also does not have information about the target, that it cannot obtain from its sensors. The leader had an average error of 26.28 m and a standard deviation of 9.08 m, while the follower airships had an average of position error of 34.60 m and a standard deviation of 3.40 m. The error distribution from the followers is shown on Figure 5.18

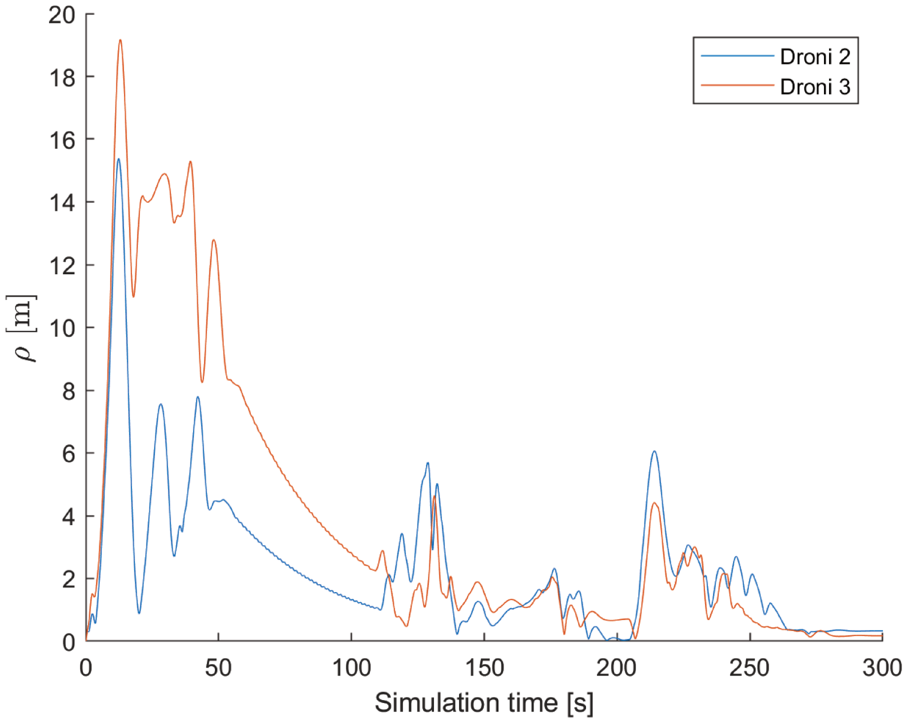

Figure 5.14 Error plot of the follower airships in Waypoint/Hovering mission (Figure 5.13). The average of the combined error is 4.61 m and the standard deviation 4.94 m.

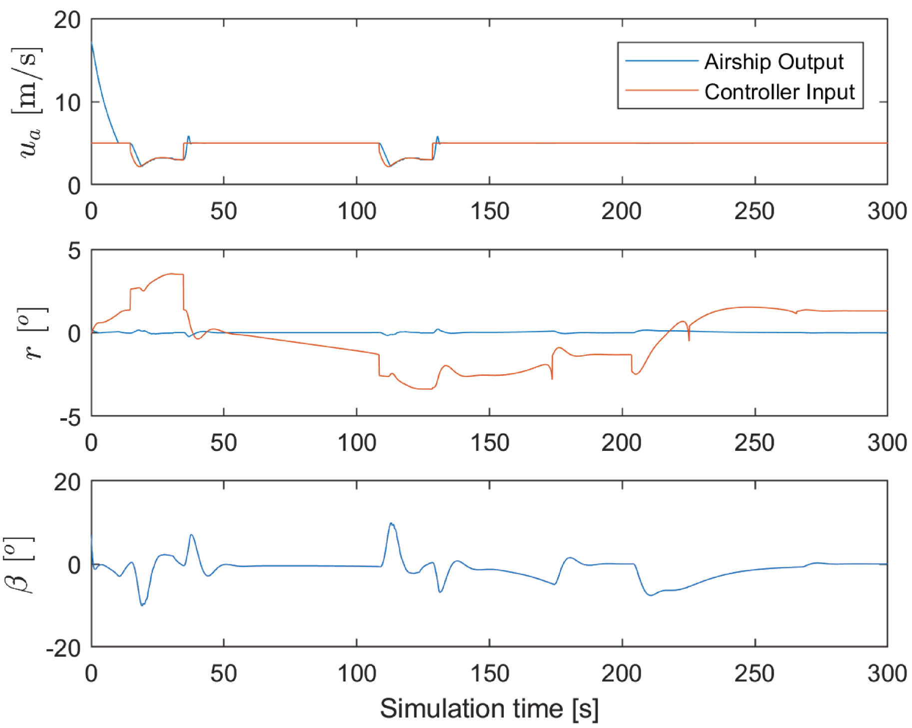

Figure 5.15 Leader's control signals and attack angle (β) during Waypoint/Hover mission (Figure 5.13).

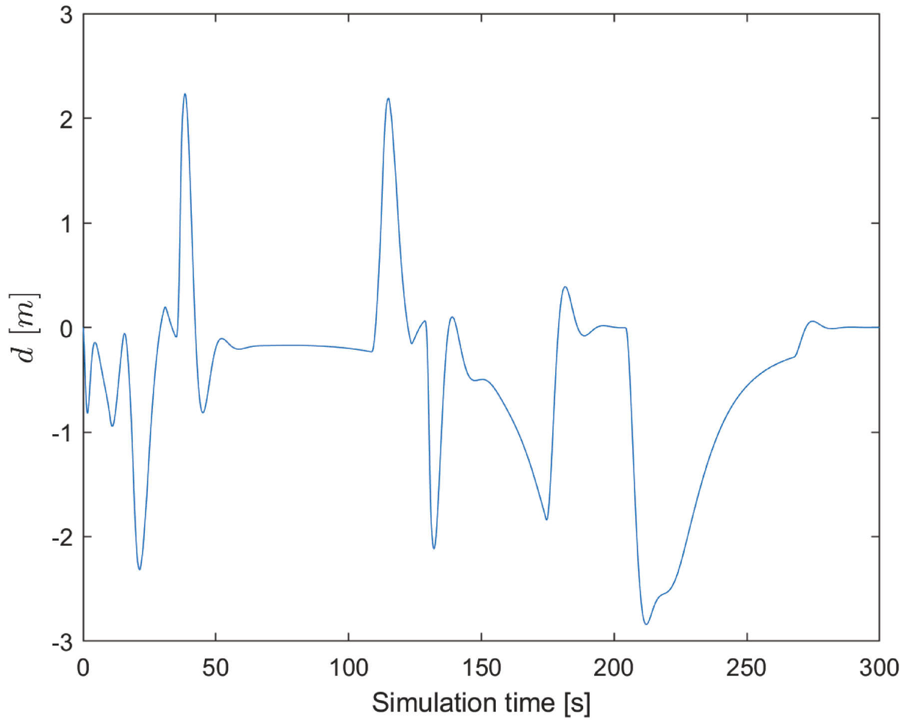

Figure 5.16 Leader's lateral error signal (d) during Waypoint/Hover mission (Figure 5.13).

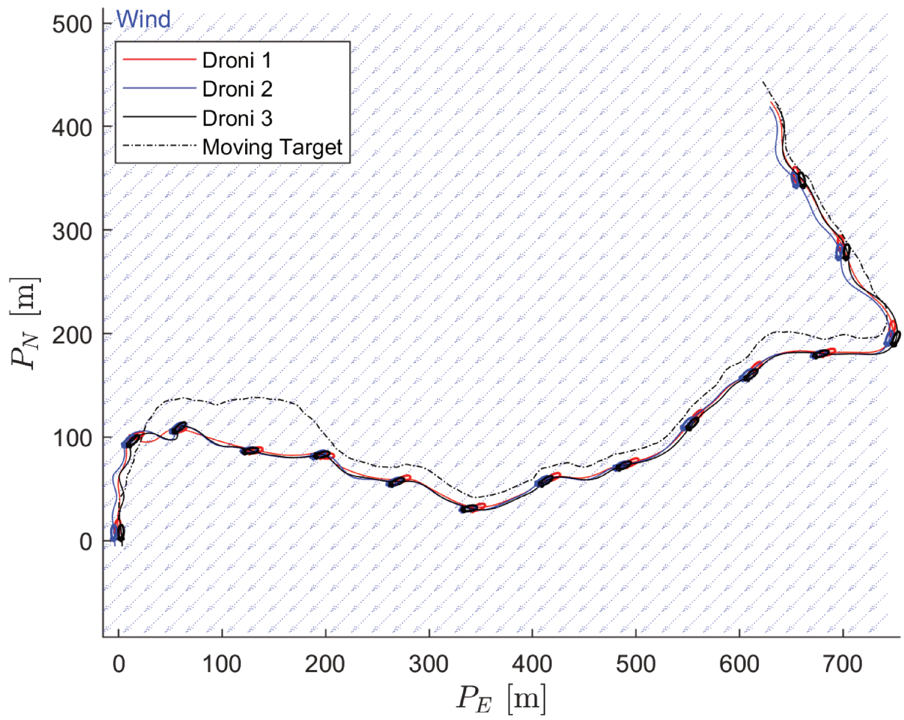

Figure 5.17 Airships in target tracking mission. The airships are drawn every 20 seconds. There was an average error of the distance between the follower airships and their reference positions of 34.60 m and a standard deviation of 3.40 m.

and from the leader is shown on Figure 5.20.

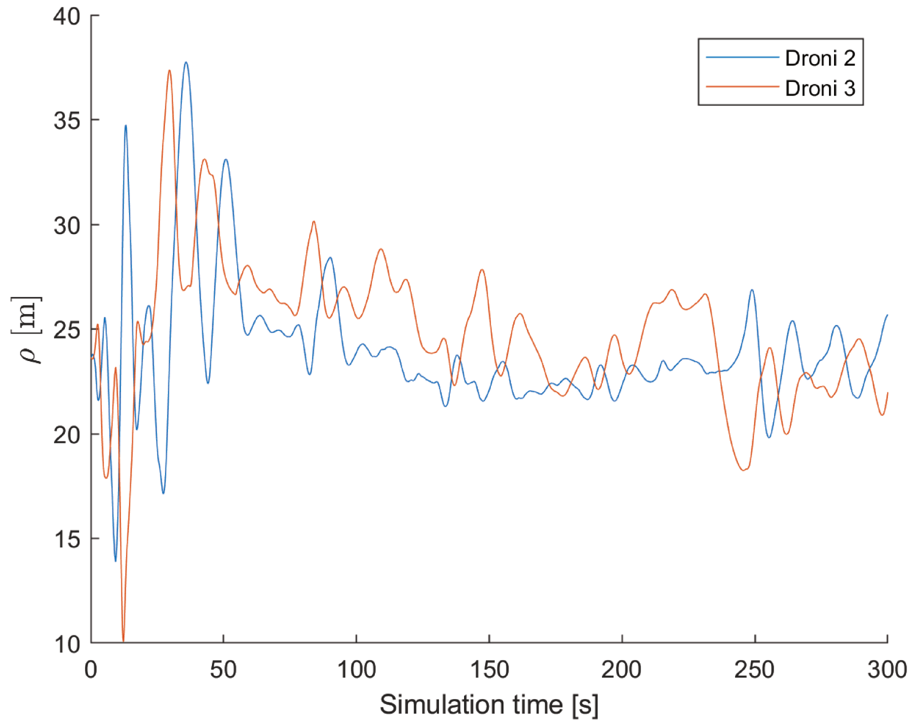

Figure 5.18 Error plot of the follower airships in moving target mission (Figure 5.17). The average of the combined error is 34.60 m and the standard deviation 3.40 m.

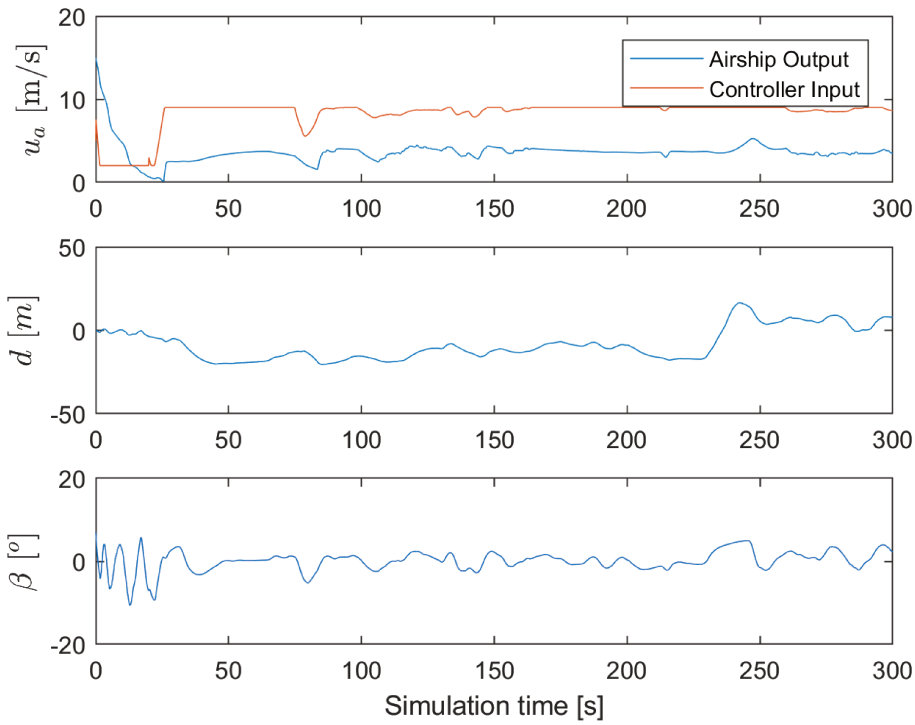

Figure 5.19 Leader's control signals and attack angle (β) during target tracking (Figure 5.17).

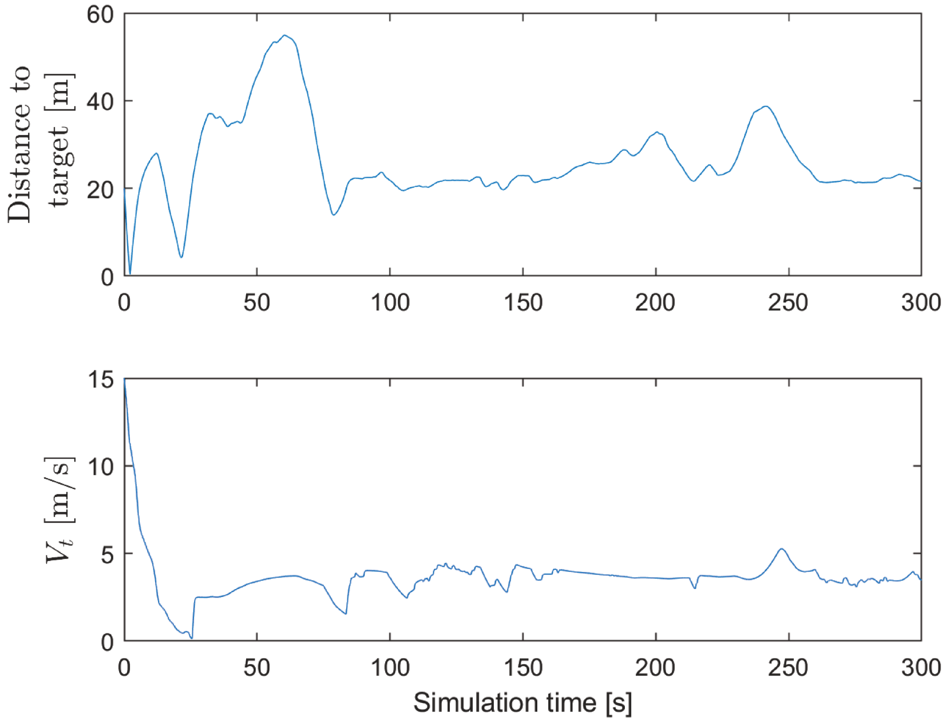

Figure 5.20 Leader's error and total velocity signals during target tracking (Figure 5.17). Its average error to the target was 26.28 m with a standard deviation of 9.08 m

6 CONCLUSIONS

It was stated in the introduction, airships have a wide range of possible applications in the monitoring and data collecting area, due to their balanced speed/cost ratio, a consequence of their aerostatic lift. With a reduced operation cost, the use of multiple airships to increase the robustness and time efficiency of the mission becomes a possibility, and often desirable.

This work presented the design of a new kind of guidance/control system for the formation flight of multiple outdoor airships that are able to perform two kinds of missions: waypoint path-following and ground-moving target tracking. It was proposed here a decentralized, three layer, hierarchical approach including mission, guidance and control layers. The guidance layer is based on the leader-follower proposal of Bicho *et al.* (2006), that is extended here to cope with more complex flight mission cases like hovering flight and ground moving tracking. The second layer controller is a state feedback kinematic controller acting on position/orientation and velocity of the airships.

For the initial stage of the project, an adapted kinematic model was developed and used in simulation, to test the control/guidance techniques. The simulation environment included emulation of a real airship behavior and a Dryden wind/turbulence model. The designed controller showed good results and tracking performances for both waypoint navigation and target tracking cases. And this is still more evident if we consider the complexity of this problem such as the underactuation of the airship, strong perturbations (wind/turbulence) and simultaneous tasks like keeping formation and following a target at the same time. The work done this far was presented at Brazilian Symposium on Intelligent Automation (SBAI) 2017 (Artaxo *et al.* (2017)).

Although many improvements were made between the kinematic and dynamical applications, this initial step as a minor goal was crucial to the development of this work. The dynamical simulator has a much larger number of variables which not only increased the complexity of the controller design, but also the simulation time, as a five minute mission that took ten to fifteen minutes to run on the kinematic simulator, would sometimes take over an hour on the dynamical one.

When implemented in the dynamical airship simulator, the controller became the outer loop of the airship feedback control. The initial design was not enough to stabilize the airship under the even most simple conditions, as the angular control had a poor performance when accounting for the wind. This was already expected as all previous publications of this project resorted to a lateral error state. The implementation of the lateral error fixed the airships trajectories, but was not enough, as the follower airships would often pass the leader. For the final controller it was still necessary to implement an integrator for the linear position error, which was fundamental to fix the follower airships flying in front of the leader and a feedforward velocity gain, to improve the velocity tracking of the follower airships. It was also necessary to tune each of the gains to minimize the distance errors and that took over sixty simulations, which amounts to approximately sixty hours of simulation.

The third layer controller, despite being out of the scope of this work which was only the second layer, also had a change in implementation. The original SMC, implemented by Vieira *et al.* (2017) worked with only one set of gains, tuned for airspeed $V_t = 5\,\mathrm{m/s}$. Due to poor performance with target tracking, where speed varied greatly in small periods of time, a scheduler was added. At each instant, the scheduler will choose the trim point closest to the actual flight conditions, which corresponds to a set of gains for the SMC. This gain scheduler for the SMC is a planned work in the context of the DRONI project, but was crudely implemented here to attend the needs of the present dissertation. Despite that, it shows the viability of such controller.

Despite the increased complexity, the dynamical model also showed good results in both waypoint/hovering navigation and ground target tracking, in some aspects, such as path deviation during waypoint flight, better results than the kinematic implementation.

As a continuation of this work, obstacle avoidance is one of the first objectives to be accomplished. With that, it will be possible to fly the airships at the same altitude without collision. Another natural extension is a complete longitudinal controller, to coordinate the airships not only horizontally, but also vertically, allowing them to realize a complete mission (take off, hover flight, cruise flight and landing) together. Finally, as the airships are pursuing the same objective, a sensorial fusion would further improve overall robustness of the mission.

BIBLIOGRAPHY

ARIAS, Ronald Ricardo. **Modelagem de um dirigível robótico com propulsão elétrica de quatro motores.** 2014. Master's thesis. Universidade Estadual deCampinas.

ARTAXO, P.G.; SARDINHA, H.; DE PAIVA, E.C.; BOURGOIS, A.; FIORAVANTI, A.R.; VIEIRA, H.S.; CORNE, D.W. e VARGAS, P.A. Control of multiple airships for autonomous surveillance and target tracking. **XIII Simpósio Brasileiro de Automação Inteligente**, volume 13, 771–778, 2017.

AZINHEIRA, J.R.; DE PAIVA, E.C. e BUENO, S.S. Influence of Wind Speed on Airship Dynamics. **Journal of Guidance, Control, and Dynamics**, volume 25, no. 6, 1116–1124, nov 2002.
URL: *http://arc.aiaa.org/doi/10.2514/2.4991*

AZINHEIRA, J.R.; DE PAIVA, E.C.; CARVALHO, J.R.H.; RAMOS, J.J.G.; BUENO, S.S.; BERGERMAN, M. e FERREIRA, P. Lateral/directional control for an autonomous, unmanned airship. **Aircraft Engineering and Aerospace Technology**, volume 73, no. 5, 453–459, oct 2001.
URL: *http://www.emeraldinsight.com/doi/10.1108/EUM0000000005880*

AZINHEIRA, J.R.; MOUTINHO, A. e CARVALHO, J.R.H. Lateral Control of Airship with Uncertain Dynamics using Incremental Nonlinear Dynamics Inversion. **IFAC-PapersOnLine**, volume 48, no. 19, 69–74, 2015.
URL: *http://dx.doi.org/10.1016/j.ifacol.2015.12.012*

AZINHEIRA, J.R.; MOUTINHO, A. e DE PAIVA, E.C. Airship Hover Stabilization Using a Backstepping Control Approach. **Journal of Guidance, Control, and Dynamics**, volume 29, no. 4, 903–914, jul 2006.
URL: *http://arc.aiaa.org/doi/10.2514/1.17334*

AZINHEIRA, J.R.; MOUTINHO, A. e DE PAIVA, E.C. A backstepping controller for path-tracking of an underactuated autonomous airship. **International Journal of Robust and Nonlinear Control**, volume 19, no. 4, 418–441, mar 2009.
URL: *http://doi.wiley.com/10.1002/rnc.1325*

BENJOVENGO, F.P.; DE PAIVA, E.C.; BUENO, S.S. e FERREIRA, P. Sliding Mode Control Approaches for an Autonomous Unmanned Airship. In **18th AIAA Lighter-Than-Air Systems Technology Conference**, May, page 13082. American Institute of Aeronautics and Astronautics, Reston, Virigina, may 2009. ISBN 978-1-62410-158-8.
URL: *http://arc.aiaa.org/doi/10.2514/6.2009-2869*

BICHO, E.; MOREIRA, A.; DIEGUES, S.; CARVALHEIRA, M. e MONTEIRO, S. Airship formation control. In **3rd International Conference on Informatics in Control, Automation and Robotics - Workshop on Multi-Agent Robotic Systems (MARS 2006)**, pages 22–33. 2006. ISBN 972886566X.
URL: *http://hdl.handle.net/1822/19247*

BUENO, S.S.; AZINHEIRA, J.R.; RAMOS, J.J.G.; DE PAIVA, E.C.; RIVES, P.; ELFES, A.; CARVALHO, J.R.H. e DA SILVEIRA, G.F. Project AURORA: Towards an Autonomous Robotic Airship. In **Proceedings of the Workshop WS6 Aerial Robotics**, pages 43–54. 2002.
URL: *https://www.researchgate.net/publication/228518304_Project_AURORA_Towards_an_autonomous_robotic_airship*

CARVALHO, J.R.H.; BUENO, S.S. e MODESTO, J.F. Sistemas Aéreos Não-tripulados para o Monitoramento e Gestão de Risco do Bioma Amazônico. **Revista Computação Brasil**, pages 145 – 154, 2014.

COLOZZA, A. e DOLCE, J. Initial feasibility assessment of a high altitude long endurance airship. **NASA Center for Aerospace Information**, , no. CR-2003-212724, 2003.
URL: *https://ntrs.nasa.gov/archive/nasa/casi.ntrs.nasa.gov/20040021326.pdf*

DE PAIVA, E.C.; AZINHEIRA, J.R. e BUENO, S.S. Controle de trajetória para veículos

terrestres de exterior. **XVIII Congresso Brasileiro de Automática - CBA2010**, 2010.
URL: *https://www.researchgate.net/publication/267229838_CONTROLE_DE_TRAJETORIA_PARA_VEICULOS_TERRESTRES_DE_EXTERIOR*

DE PAIVA, E.C.; AZINHEIRA, J.R. e MOUTINHO, A. Erratum on "Influence of Wind Speed on Airship Dynamics". **Journal of Guidance, Control, and Dynamics**, volume 31, no. 2, 443–444, mar 2008.
URL: *http://arc.aiaa.org/doi/10.2514/1.33409*

DE PAIVA, E.C.; AZINHEIRA, J.R.; RAMOS, J.J.G.; MOUTINHO, A. e BUENO, S.S. Project AURORA: Infrastructure and flight control experiments for a robotic airship. **Journal of Field Robotics**, volume 23, no. 3-4, 201–222, mar 2006.
URL: *http://dx.doi.org/10.1002/rob.20111*

DE PAIVA, E.C.; BENJOVENGO, F.P. e BUENO, S.S. Sliding mode control for the path following of an unmanned airship. **IFAC Proceedings Volumes (IFAC-PapersOnline)**, volume 6, no. PART 1, 221–227, 2007.
URL: *http://linkinghub.elsevier.com/retrieve/pii/S1474667016346651*

FLINT, M.; POLYCARPOU, M. e FERNANDEZ-GAUCHERAND, E. Cooperative control for multiple autonomous UAV's searching for targets. In **Proceedings of the 41st IEEE Conference on Decision and Control, 2002.**, volume 3, pages 2823–2828. IEEE, IEEE, 2002. ISBN 0-7803-7516-5.
URL: *http://ieeexplore.ieee.org/document/1184272/*

GOMES, S.B.V. e RAMOS, J.J.G. Airship dynamic modeling for autonomous operation. In **Proceedings. 1998 IEEE International Conference on Robotics and Automation**, volume 4, pages 3462–3467. IEEE, 1998. ISBN 0-7803-4300-X.
URL: *http://ieeexplore.ieee.org/document/680973/*

KHOURY, G.A. Airship Technology. **Aircraft Engineering and Aerospace Technology**, jun 2012.

URL: *http://www.cambridge.org/br/academic/subjects/engineering/aerospace-engineering/airship-technology-2nd-edition?format=HB&isbn=9781107019706*

KING, E.; KUWATA, Y.; ALIGHANBARI, M.; BERTUCCELLI, L. e HOW, J. Coordination and control experiments on a multi-vehicle testbed. In **Proceedings of the American Control Conference**, volume 6, pages 5315–5320. IEEE, 2004. ISBN 0780383354.

LAMB, H. The inertia coefficients of an ellipsoid moving in fluid. **British Aeronautical Research Commitee Report and ...**, , no. 623, 3–5, 1918.
URL: *http://mararchief.tudelft.nl/catalogue/entries/9936/*

MARTON, Apolo Silva. **Controle linear de trajetória de dirigível robótico com propulsão quádrupla**. 2016. Master's thesis. Universidade Estadual de Campinas.

MORIGUCHI, Sergio Kenji. **Controle não linear de dirigíveis por Backstepping e Sliding Modes**. 2017. Ph.D. thesis. Universidade Estadual de Campinas.

MORIN, P. e SAMSON, C. Motion Control of Wheeled Mobile Robots. In **Springer Handbook of Robotics**, pages 799–826. Springer Berlin Heidelberg, Berlin, Heidelberg, 2008. ISBN 978-3-540-23957-4.
URL: *http://link.springer.com/10.1007/978-3-540-30301-5_35*

MOUTINHO, Alexandra. **Modeling and Nonlinear Control for Airship Autonomous Flight**. 2007. , no. August, 178. Ph.D. thesis. Universidade Técnica de Lisboa.
URL: *https://www.researchgate.net/publication/267567521_Modeling_and_nonlinear_control_for_airship_autonomous_flight https://doi.org/10.13140/2.1.1333.8568*

MOUTINHO, A.; AZINHEIRA, J.R.; DE PAIVA, E.C. e BUENO, S.S. Airship robust path-tracking: A tutorial on airship modelling and gain-scheduling control design. **Control Engineering Practice**, volume 50, 22–36, may 2016.
URL: *http://dx.doi.org/10.1016/j.conengprac.2016.02.009 http://linkinghub.elsevier.com/retrieve/pii/S0967066116300314*

OH, Hyondong. **Towards Autonomous Surveillance and Tracking by Multiple UAVs**. 2013. volume PhD. Ph.D. thesis. Cranfield University.

OLSEN, E.A.; PARK, C.W. e HOW, J. 3D Formation Flight Using Differential Carrier-Phase GPS Sensors. **Navigation**, volume 46, no. 1, 35–48, mar 1999.
URL: *http://doi.wiley.com/10.1002/j.2161-4296.1999.tb02394.x*

PIMENTA, L.C.A.; SCHWAGER, M.; LINDSEY, Q.; KUMAR, V.; RUS, D.; MESQUITA, R.C. e PEREIRA, G.A.S. Simultaneous Coverage and Tracking (SCAT) of Moving Targets with Robot Networks. In **Springer Tracts in Advanced Robotics**, volume 57, pages 85–99. 2009. ISBN 9783642003110.
URL: *http://link.springer.com/10.1007/978-3-642-00312-7_6*

PINAGÉ, F.A.; CARVALHO, J.R.H. e QUEIROZ-NETO, J.P. Visual-based Natural Landmark Tracking Method to Support UAV Navigation over Rain Forest Areas. In **VISAPP (2)**, pages 416–419. 2013.

RAMOS, J.J.G.; DE PAIVA, E.C.; AZINHEIRA, J.R.; BUENO, S.S.; MAETA, S.; MIRISOLA, L.; BERGERMAN, M. e FARIA, B. Autonomous flight experiment with a robotic unmanned airship. In **Proceedings 2001 ICRA. IEEE International Conference on Robotics and Automation (Cat. No.01CH37164)**, volume 4, pages 4152–4157. IEEE, 2001. ISBN 0-7803-6576-3.
URL: *http://ieeexplore.ieee.org/document/933267/*

SHANMUGAVEL, Madhavan. **Path planning of multiple autonomous vehicles**. 2007. Ph.D. thesis.

SHTESSEL, Y.; EDWARDS, C.; FRIDMAN, L. e LEVANT, A. **Sliding mode control and observation**. Control Engineering. Springer New York, New York, NY, 2014. ISBN 9780817648930.
URL: *http://link.springer.com/10.1007/978-0-8176-4893-0*

SIEGWART, R.; NOURBAKHSH, I.R. e SCARAMUZZA, D. **Introduction to Autonomous**

Mobile Robots. MIT press, 2nd edition, 2011. ISBN 9780262015356.
URL: *https://mitpress.mit.edu/books/introduction-autonomous-mobile-robots*

SMITH, T.; BINGHAM, C.; STEWART, P.; ALLARTON, R. e STEWART, J. Energy harvesting and power network architectures for the multibody advanced airship for transport high altitude cruiser–feeder airship concept. **Proceedings of the Institution of Mechanical Engineers, Part G: Journal of Aerospace Engineering**, volume 227, no. 4, 586–598, apr 2013.
URL: *http://journals.sagepub.com/doi/10.1177/0954410012469319*

STEVENS, B.L.; LEWIS, F.L. e JOHNSON, E.N. **Aircraft Control and Simulation: Dynamics, Controls Design, and Autonomous Systems**. John Wiley & Sons, Inc, Hoboken, NJ, USA, nov 2015. ISBN 9781119174882.
URL: *http://doi.wiley.com/10.1002/9781119174882*

THOMASSON, P.G. Equations of Motion of a Vehicle in a Moving Fluid. **Journal of Aircraft**, volume 37, no. 4, 630–639, jul 2000.
URL: *http://arc.aiaa.org/doi/10.2514/2.2645*

TITTERTON, D. e WESTON, J. **Strapdown Inertial Navigation Technology**, volume 3. IET, The Institution of Engineering and Technology, Michael Faraday House, Six Hills Way, Stevenage SG1 2AY, UK, jan 2004. ISBN 9780863413582.
URL: *http://digital-library.theiet.org/content/books/ra/pbra017e*

TSOURDOS, A.; WHITE, B. e SHANMUGAVEL, M. **Cooperative Path Planning of Unmanned Aerial Vehicles**. John Wiley & Sons, Ltd, Chichester, UK, nov 2010. ISBN 9780470974636.
URL: *http://doi.wiley.com/10.1002/9780470974636*

US ARMY. Long Endurance Multi-Intelligence Vehicle (LEMV) Agreement Signed. 2010.
URL: *https://www.army.mil/article/41024/long-endurance-multi-intelligence-vehicle-lemv-agreement-signed*

VIEIRA, H.S.; MARTON, A.S.; DE PAIVA, E.C.; FIORAVANTI, A.R. e BUENO, S.S. Controle de um Dirigível Robótico Autônomo de Propulsão Quádrupla Utilizando Modos Deslizantes. **XIII Simpósio Brasileiro de Automação Inteligente**, , no. October, 2017.
URL: *https://www.researchgate.net/publication/320730816_CONTROLE_DE_UM_DIRIGIVEL_ROBOTICO_AUTONOMO_DE_PROPULSAO_QUADRUPLA_UTILIZANDO_MODOS_DESLIZANTES*